UiT The Arctic University of Norway

Department of Pharmacy

# Microfluidized liposomes for cellular uptake imaging: Optimization

Silje Mork

Masteroppgave i Farmasi FAR-3911 mai 2020

# Acknowledgements

The work in this thesis was accomplished in the Drug Transport and Delivery Research Group, Department of Pharmacy, with collaboration from the Women's Health and Perinatology Research Group, Department of Clinical Medicine, Faculty of Health Sciences and the Advanced Microscopy and Imaging facilities at University of Tromsø - The Arctic University of Norway, Tromsø, from October 2019 to May 2020. I have to say that for this opportunity I am beyond grateful to everyone that I have either worked with or has otherwise helped me in this time. I most certainly could not have done this without you.

First, I would like to express my gratitude towards my supervisors PhD student Jennifer Cauzzo and Professor Nataša Škalko-Basnet. Nataša has my appreciation for giving me an interest in this field and topic. Thank you for your advice and encouragement. To Jennifer, I would like to recognize the invaluable assistance you have provided me during my study. You have inspired in me an irreplaceable work ethic, and I am very grateful to have had you as my supervisor and for all you have done for me.

I would like to show my respect for the Drug Transport and Delivery Research Group. Never have I experienced such a supportive, kind and engaging group of people. You gave me motivation in my work, and I knew that if I ever had some questions, I could always ask. Thank you for making me feel welcome. Then I would also like to use this opportunity to show gratitude towards Professor II Purusotam Basnet and the Women's Health and Perinatology Research Group. Thank you for welcoming me into your facility and giving me guidance in a new field. I too wish to thank Roy A. Lysså at the Advanced Microscopy and Imaging facilities, for his accommodating assistance. Special thanks also to Cristiane De Albuquerque Cavalcanti Jacobsen for taking care of me and my peers in the laboratory, and to PhD student Lisa Myrseth Hemmingsen for her advice. To my laboratory peers, Ann Kristin Pettersen, Julie Olussen, Kasi Shorsh, Luqman Ahsan and Sunniva Brurok, thank you, your help and company in the lab has been much appreciated.

I also wish to acknowledge the support from another fellow peer whom I shared work space with, Andrea Barnie Antobreh for your continued support and encouragement. Your daily company during lunch breaks and long work days are invaluable to me, thank you for your humor and lifting my days. Also great love to my family, especially my mother, Janne P. K.

Mork for her continued vocal support and my father, Tore Mork for always bringing reassurance. They kept me going, thank you for your thoughts.

Tromsø, 10.05.2020

# Table of Contents

# List of Tables



## Appendix

# List of Figures

## Appendix

# Abbreviations

| | |
|---|---|
| $^{31}$P NMR | Phosphorus Nuclear Magnetic Resonance |
| DC | Dual Centrifugation |
| dH2O | Distilled Water |
| DLS | Dynamic Light Scattering |
| DMSO | Dimethyl sulfoxide |
| DPSE-PEG | 1,2-distearoyl-sn-glycero-3-phosphoethanolamine-N-[methoxy(polyethylene glycol)-2000] |
| EPR | Enhanced Permeability and Retention |
| EtOH | Ethanol |
| FACS | Fluorescence Activated Cell Sorting |
| FSC | Forward Scatter |
| IC | Intersystem Crossing |
| IFC | Imaging Flow Cytometry |
| iNOS | Inducible Nitric Oxide Synthase |
| ISC | Inter System Crossing |
| LPS | Lipopolysaccharide |
| LUV | Large Uni-lamellar Vesicle |
| MeOH | Methanol |
| MHF | Micro Hydrodynamic Focusing |
| MLV | Multi Lamellar Vesicle |
| MVV | Multi Vesicular Vesicle |

| | |
|---|---|
| NO | Nitric Oxide |
| PCS | Photon Correlation Spectroscopy |
| PDI | Polydispersity Index |
| PEG | Polyethylene Glycol |
| RES | Reticuloendothelial System |
| SD | Standard Deviation |
| SSC | Side scatter |
| SUV | Small Uni-lamellar Vesicle |
| ULV | Uni-lamellar Vesicle |
| VPG | Vesicular Phospholipid Gel |

## Sammendrag

Liposomer som medikamentleveringssystemer utviser stort potensiale for å levere aktive molekyler til det målrettede stedet avhengig av deres forskjellige egenskaper som størrelse, overflateegenskaper og medikamentbelastning. Imidlertid er disse karakteristikkene avhengige av fremstillingsprosedyrene som brukes for å fremstille liposomer. Spesielt vanskelig er forsikring om reproduserbar produksjon i store volum, noe som hevdes å være nødvendig for farmasøytisk produksjon. Derfor er det nødvendig med en rask og effektiv skalerbar metode for produksjon av liposomer. Høyttrykkshomogenisering ved bruk av en mikrofluidisator har vist å være i stand til å fremstille store volum liposomer, men det finnes ikke en enkel oppsetting på denne maskinen som garanterer reproduserbare formuleringer. For en slik metode er undersøkelse av liposom-karakteristika viktig, og ved å legge fluoroforer i formuleringen så øker mulighetene til å følge både egenskaper og skjebne av liposomer i organismer via avbildning. Andre fordeler med fluorescerende liposomer er fordelene de gir ved avbildning, men skal resultatet være nyttig og pålitelig, må fluorescerende liposomer imidlertid ha samme oppførsel som det vanlige liposomet. Derfor må fluoroforen forbli innkapslet i liposomene for å muliggjøre undersøkelsesprosessen av biologiske hendelser som internalisering av liposomer av celler.

Målet med dette prosjektet var å optimalisere mikrofluidiseringsparametere for produksjon av fluorescerende liposomer for celleopptaksbilding og biologisk aktivitetstesting på cellekulturer. En del av optimaliseringsprosessen var å observere hvordan forskjellige tilsatte molekyler påvirket prosesseringen og egenskapene til prosesserte liposomer. Liposomene ble fremstilt ved å bruke tynnfilmhydratisering og deretter prosessering med en LM20 mikrofluidisator. Tre forskjellige komponenter ble tilsatt lipidene i separate formuleringer, nemlig rodamin B, gurkemeie og PEG. Liposomene ble karakterisert og sammenlignet. Den antiinflammatoriske aktiviteten til gurkemeie liposomer ble undersøkt *in vitro* i lipopolysakkarid-inflammerte makrofager (RAW 264.7) ved å måle nitrogenoksid-produksjon. Disse cellene ble deretter undersøkt for fluorescens og avbildet i flytcytometri.

Rodamin B liposomer var polydisperse med to størrelse topper på 15 og 171 nm og hadde et kationisk zeta-potensial. Gurkemeie liposomer ble funnet å være homogene med en gjennomsnittlig størrelse på 76 nm og et nøytralt zeta-potensial. PEGylerte liposomer var også homogene med en størrelse på 174 nm og viste et anionisk zeta-potensiale. Homogene

formuleringer var stabile over testet tidsperiode (60-90 dager). Cellulært opptak av gurkemeie liposomer kunne ikke visualiseres.

Optimaliseringen av liposomer for mikrofluidisering må utføres for hver liposomale sammensetning, da noen komponenter er gunstige og andre skadelige for de liposomale egenskapene. Å øke viskositeten til suspensjonen og/eller membranstivheten synes å være fordelaktig. Stabile formuleringer kan fremstilles, og ytterligere avbildningsoptimalisering kan potensielt avsløre mekanismene bak internalisering for liposomal gurkemeie.

## Abstract

Liposomes as drug delivery systems exhibit great potential to deliver active molecules to the targeted site depending on their various characteristics such as size, surface properties and drug/active molecule load. However, these characteristics are dependent on the manufacturing procedures applied to prepare liposomes. Especially difficult is assurance of reproducible production in large volumes, which is argued to be necessary for pharmaceutical production. Therefore a fast and efficient up-scalable method for production of liposomes is needed. High pressure homogenization utilizing a microfluidizer has shown to be able to prepare large volumes of liposomes, however there is not an easy set up on this machine that guarantees reproducible formulations. For such a method, screening of the liposomes characteristics are important, moreover adding fluorophores to liposomes increases the ability to follow both their characteristics and fate in organisms via imaging. Other benefits of fluorescently labeled liposomes is the benefits it provides in imaging. However for the result to be useful and reliable, fluorescently labeled liposomes must exhibit the same behavior as the plain liposome. Therefore, the fluorophore must stay encapsulated within liposomes to enable the screening process of biological events such as internalization of liposomes by cells.

The aim was to optimize microfluidizer parameters for the production of fluorescent liposomes for cell uptake imaging and biological activity testing on cell cultures. Part of the optimization process was to observe the way the various added molecules affected the processing and the characteristics of processed liposomes. The liposomes were prepared using thin film hydration and then processed with an LM20 Microfluidizer. Three different components were added to lipids in separate formulations, namely rhodamine B, curcumin and PEG. The liposomes were characterized and compared. The anti-inflammatory activity of curcumin liposomes were investigated *in vitro* in lipopolysaccharide-inflamed macrophages (RAW 264.7) by measuring the nitric oxide production. These cells were then screened for fluorescence and imaged in flow cytometry.

Rhodamine B liposomes were polydisperse with two mean size peaks at 15 and 171 nm and had a cationic zeta-potential. Curcumin liposomes was found to be homogeneous with a mean size peak at 76 nm and a neutral zeta-potential. PEGylated liposomes were also homogeneous with a size of 174 nm exhibiting an anionic zeta-potential. Homogenous formulations were stable over tested period of time (60-90 days). The cellular uptake of curcumin liposomes could not be visualized.

The optimization of liposomes for microfluidization needs to be performed for each liposomal composition, because some components are beneficial and others detrimental to liposomal characteristics. Increasing the viscosity of suspension and/or membrane rigidity seems to be beneficial. Stable formulations can be prepared, and further imaging optimization could potentially reveal the mechanisms behind internalization behind liposomal curcumin.

# 1 Introduction

For any drug, its therapeutic potential is determined by how effective it is at its given task (treatment, imaging and diagnosis, etc.). However this can be argued to be mediated by how much drug reaches its intended target. A lot of pharmaceutical active ingredients are hindered by poor pharmacokinetics, something that potentially impedes their therapeutic activity in the body. One way to improve the pharmacokinetics of a drug, is through drug delivery systems (Patra et al., 2018).

Some drug delivery systems include carrier systems that can be made from a variety of different materials. These materials can be in the nanoscale (<1 µm), something that is beneficial because of nanomaterials unique characteristics. These carriers are referred to as nanocarriers. Due to their small size, they not only provide a large surface area, but also the ability to overcome biological barriers like epithelial and endothelial cells, as well as cell membranes (Pastorino et al., 2019). This is beneficial as it provides good pharmacokinetic properties such as increased absorption (where applicable) and bioavailability. As such, encapsulating drug in a carrier gives a potential to increase the pharmacokinetics of the entrapped drug (Patra et al., 2018).

Nanocarriers made from lipids offer several different ways to overcome problems in drug delivery and are as such preferable nanocarriers used in nanomedicine. One such highly utilized carrier are liposomes (Sercombe et al., 2015). Liposomes can have different characteristics and each characteristic can be tailored according to the intended use of the final formulation. These characteristics can be the size, surface charge or membrane rigidity. There are many different ways of providing the liposomes with their desirable characteristics, however liposomes can be difficult to manufacture in reproducible manner, especially in larger volumes as needed for industrial pharmaceutical production (Sercombe et al., 2015; Evers et al., 2018). One way to size reduce large volumes of liposomes is through high pressure homogenization with a microfluidizer. This machine can process large volumes at a time, and as such is appealing to use in industry (Schuh et al., 2018).

## 1.1 Liposomes

Liposomes are small, spherical vesicles that consist primarily of non-toxic amphiphilic phospholipids (Monteiro et al., 2014; Sercombe et al., 2015). The phospholipids arrange into lipid bilayers, creating both a lipophilic space in the lipid bilayer and an aqueous space in the core and between bilayers. Therefore liposomes can entrap both lipophilic and hydrophilic compounds. The lipophilic will be located in the lipid bilayer, and the hydrophilic in the aqueous space. This means that a wide variety of drugs as well as other molecules like DNA, imaging agents or proteins can be entrapped in liposomes (Sercombe et al., 2015; Eroğlu & İbrahim, 2020). Liposomes can also contain many other components such as cholesterol, and their characteristics change depending on which components are used. The characteristics such as the surface charge, size or membrane rigidity are of most interest (Akbarzadeh et al., 2013; Eroğlu & İbrahim, 2020).

Liposomes exhibit good biocompatibility, something that means that they are not likely to cause toxic, immunogenic or other adverse effects in the body. This is likely due their ability to mimic naturally occurring cell-membranes as both are composed of phospholipids in a bilayer formation. Their compatibility coupled with the advantageous loading ability make liposomes useful as drug delivery systems (Bozzuto & Molinari, 2015; Sercombe et al., 2015; Dos et al., 2018).

Entrapping drug or other molecules inside of liposomes has several advantages. The encapsulation inside of a lipid bilayer can protect the drug from naturally occurring harmful conditions. This can be the prevention of early biodegradation and inactivation by protecting it from enzymes, or increase the circulation time by helping the payload avoid the immune system. They can also simultaneously reduce toxicity of toxic drugs/molecules due to minimizing the exposure time to non-target tissue. Other advantages include the improved absorption, distribution and elimination of drugs with poor pharmacokinetics (Bozzuto & Molinari, 2015; Amreddy et al., 2019). Liposomes are also rather easy to prepare in laboratories from a variety of lipids (Monteiro et al., 2014).

### 1.1.1 Types of liposomes

A drug or molecule that does not reach the target will not have therapeutic effect. This can be a drawback for liposomal formulations as liposomes can exhibit low stability, a short circulation

time and leak their content through diffusion or breaks in the bilayer. If the encapsulated drug/molecule does not reach its intended target, the formulation cannot be considered as having good efficacy (Monteiro et al., 2014; Amreddy et al., 2019).

To improve these potential drawbacks liposomes can among other things, undego some modifications to their surface or bilayer. Their size also varies between 20 nm to several µm. Liposomes can therefore be different from each other, and are classified based on a number of different characterizations. This can be the surface modifications, number of lamellae, size or materials used during preparation. Formulations of liposomes differ regarding the mentioned characteristics (Sercombe et al., 2015; Amreddy et al., 2019).

If the classification is based on their size and number of lipid bilayers, liposomes may be placed in three main categories. These are multi lamellar vesicles (MLVs), multi vesicular vesicles (MVVs) and uni-lamellar vesicles (ULVs) (Figure 1) (Kanasova & Nesmerak, 2017).

MLVs are generally large vesicles with multiple layers of lipid bilayers. MVVs are similar to MLVs however this type has several smaller vesicles encapsulated inside the different lipid bilayers. ULVs are generally smaller than both MLVs and MVVs with a size between 20 and 500 nm and are generally split into two subcategories; Large uni-lamellar vesicles (LUVs, >100 – 500 nm) and small uni-lamellar vesicles (SUVs, 20 – 100 nm). These have only one lipid bilayer and are usually prepared from MLVs via size reduction (Monteiro et al., 2014; Kanasova & Nesmerak, 2017).

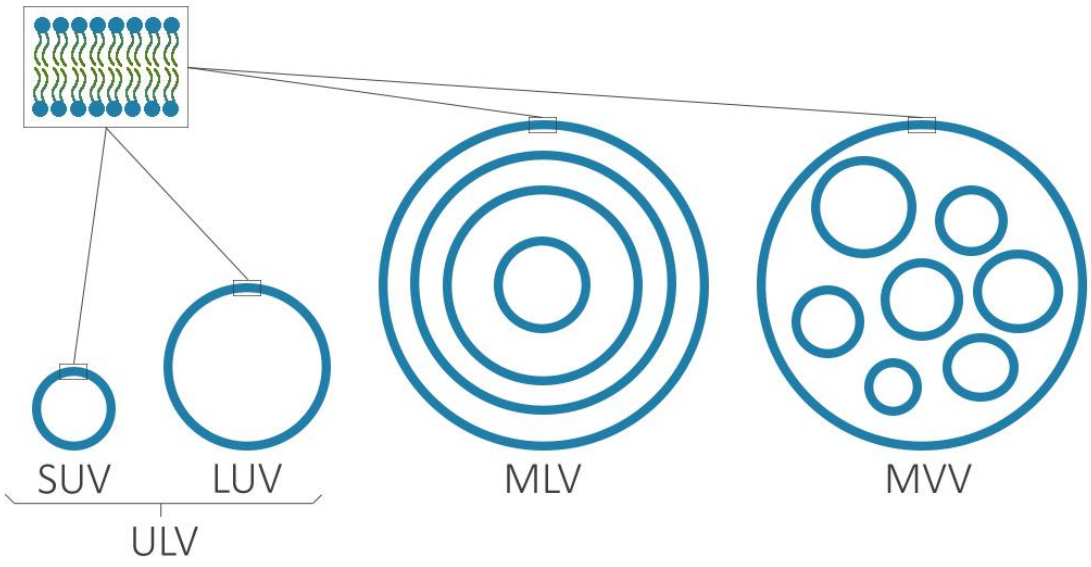


***Figure 1:*** *Representation of liposomal types based on lamellarity and size. Figure adapted from (Monteiro et al., 2014; Kanasova & Nesmerak, 2017).*

Other ways to classify liposomes are based on their surface modifications. Some of these categories include conventional liposomes, sterically-stabilized liposomes and targeted liposomes, including combinations of these (Bansal et al., 2011; Sercombe et al., 2015).

Conventional liposomes were the first type of liposome developed and are liposomes without any surface modifications (Sercombe et al., 2015). Later iterations of conventional liposomes are emerging, some with modifications to their membrane. One such type of conventional liposome is called deformable liposomes also known as transfersomes. This type of liposome has in addition to phospholipids, an edge activator (biocompatible surfactant) that increases the flexibility of their lipid bilayer membrane. This makes for extremely flexible and elastic liposomes without compromising on the liposomes beneficial structure. These deformable liposomes are often used in topical formulations, as they have shown superior ability to penetrate into deeper skin layers than other conventional liposomes (Lu et al., 2019; Ternullo et al., 2019). Other types of modifications of the liposomes membrane includes tailoring their bilayer rigidity or fluidity. This is done for several reasons, especially to make them resistant to leaking of their entrapped content (Wu et al., 2019).

A disadvantage with conventional liposomes is their short circulation time because of their fast elimination from the bloodstream. The elimination is due to opsonization by the reticuloendothelial system (RES), such as the spleen and liver. This limits the therapeutic efficacy of these liposomes, and may be unwanted for a drug-delivery system (Zahednezhada et al., 2019).

Sterically-stabilized liposomes were developed to prevent this rapid elimination. These are liposomes that have polymer chains attached to their surface, providing them some new characteristics. These polymer chains are often used to stabilize and protect liposomes from RES detection to increase their circulation time. Because of this, sterically-stabilized liposomes are often referred to as stealth liposomes (Figure 2, p. 5) (Zahednezhada et al., 2019).

Polyethylene glycol (PEG) is a biocompatible hydrophilic polymer that has shown to achieve sterically-stabilized liposomes and increase their circulation time. PEG has also shown to have mucus-penetrating abilities by eliminating adhesive interactions between liposomes and mucus, making way for mucus penetrating liposomes (Monteiro et al., 2014; Jøraholmen et al., 2017). Surface modifications with polymers such as chitosan can lead to mucoadhesive liposomes. Chitosan coated liposomes have good adhesive properties that can potentially increase the

efficacy of localized therapy. This due to the increased exposure time to localized tissue (Hea et al., 2019).

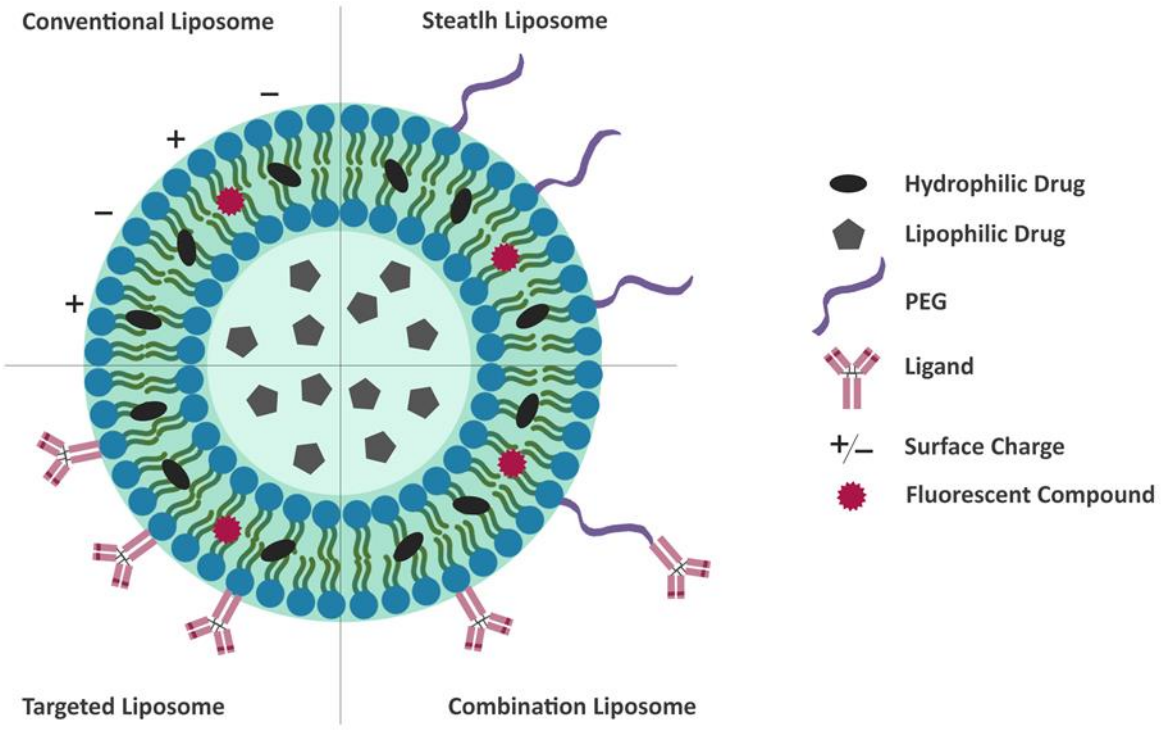


***Figure 2**: Representation of different types of surface modified liposomes. Figure adapted from (Sercombe et al., 2015; Hea et al., 2019).*

Liposomes that manage to avoid opsonization by the RES, like sterically stabilized liposomes are ideal for passive drug targeting. This is because passive targeting utilizes the Enhanced Permeability and Retention (EPR) effect (Sercombe et al., 2015; Zahednezhada et al., 2019). The EPR effect describes the effect that fast growing tumors have on surrounding endothelial cells. This effect gives the endothelial cells larger than normal gap junctions that enable the passage of liposomes which is limited in normally much tighter junctions. Liposomes can utilize this for tumor targeting due to their small size (Eroğlu & İbrahim, 2020).

For active targeting, targeted liposomes were developed. These are liposomes that have gone through a surface modification to improve their distribution pattern using e.g. ligands like monoclonal antibodies, other antibodies, enzymes or other proteins, and much more (Figure 2). This type of liposome therefore has the ability to target specific targets and can deliver their payload to specific sites that e.g. overexpresses certain types of ligands. Targeted liposomes can also utilize the EPR effect and have the same disadvantage as conventional liposomes, their limited circulation time due to the RES. This is the reason that most actual liposomal

formulations use a combination of different types of surface and/or bilayer modifications (Figure 2, p. 5) (Sercombe et al., 2015; Zahednezhada et al., 2019).

### 1.1.2 Liposome preparation

There are several ways to prepare liposomal formulations, most of these can be divided into two main categories, film methods and bulk methods. The film methods involve the preparation of a lipid film that is then rehydrated into liposomes using an aqueous media. The bulk methods involve the dissolving of lipids into organic solvents and the transfer of that solution into aqueous media to form liposomes. Two commonly used methods for liposomal preparation are the thin film hydration method (film) and the ethanol injection method (bulk). Even though the methods for liposome preparation are different, they all share the same four main principals of preparation (Patil & Jadhav, 2013; Has & Sunthar, 2019).

1. Dissolving the lipids in an organic solvent
2. Removing the solvent in exchange for an aqueous medium
3. Processing the liposomes to get the desired characteristics
4. Analyzing the liposomes

How these four stages are performs is what makes the processes differ from each other (Akbarzadeh et al., 2013). There are also some newer preparation methods that e.g. utilizes microfluidics technology (Patil & Jadhav, 2013; Has & Sunthar, 2019). Other newer methods of preparing liposomes merge the first three steps, such as the “one-step” preparation method and the dual centrifugation, and also do not require solvents (Brandl, 2007; Ingebrigtsen et al., 2017).

#### 1.1.2.1 Thin film hydration

In the thin film hydration method, the lipids are first dispersed in an organic solvent, which is then removed using a rotary evaporator (rotavapor). This forms a thin lipid film that is then rehydrated using a suitable aqueous medium. After the addition of the medium, liposomes will start to self-assemble, and by shaking or otherwise keeping the mixture under movement, the liposomes will be dispersed in the medium. The shaking should continue until the film is completely rehydrated and dislodged. This should result in a homogeneous liposomal dispersion. However while homogenous, the liposomes will be rather large, up to µm in size,

and generally a size reduction process is needed after the thin film hydration to assure liposomes of preferred size for drug delivery (Monteiro et al., 2014; Has & Sunthar, 2019).

#### 1.1.2.2 Ethanol injection

In this method of liposome preparation, lipids are first dissolved in ethanol. This solution of lipids and ethanol is then dropwise injected into an aqueous solution (water, buffer etc.). This forces the lipids out of solution, which makes them self-assemble into liposomes. This method is capable of creating SUVs without further size reduction, however the system may not be homogeneous. The size has been shown to depend on the drop size and lipid concentration, and will likely still need a size reduction (Patil & Jadhav, 2013; Has & Sunthar, 2019).

#### 1.1.2.3 Microfluidic methods

Microfluidics is the process of controlled fluid flow in channels with cross sectional dimensions (5-500 μm). This is not the same as using a microfluidizer, as that machine utilizes high pressure. Microfluidics when producing liposomes can lead to homogeneous ULVs as it has good size control, however size has shown to be somewhat reliant on the phospholipid concentration. One such microfluidic liposome method is through Micro Hydrodynamic Focusing (MHF). Here an aqueous solution (e.g. buffer) flows in a controlled stream along two opposite walls of a channel. Then a phospholipid solution in alcohol flows in the middle of the channel. Due to counter diffusion of water and alcohol, the lipids are forced to self-assemble into bilayers, and these eventually close and form liposomes (Patil & Jadhav, 2013; Has & Sunthar, 2019).

#### 1.1.2.4 One-step liposome preparation

Another method for the preparation of liposomes includes a “one-step” preparation technique where a mixture of dried phospholipids and an aqueous liquid (buffer, drug solution etc.) is added together into a microfluidizer. This can result in small finely dispersed lipid particles, which will swell and self-assemble into liposomes. However, the lipid to liquid ratio and the composition of the lipid phase are parameters important to optimize, as the result of this method may not always be vesicle formation. This method also does not necessarily make a normal liposomal dispersion, even if vesicles are achieved. Instead a vesicular phospholipid gel (VPG) is obtained in its stead. VPGs are dense, cream like dispersions with very little space between

the vesicles due to a low liquid to lipid concentration. These VPGs can be diluted to a conventional SUV dispersion using a suitable aqueous solution. This method is called one step, as the preparation and processing can be done in one single step, however characterization is still necessary afterwards (Brandl, 2007).

#### 1.1.2.5 Dual Centrifugation

A newer method of preparing liposomes is through dual centrifugation (DC), where a sample container with e.g lipids and medium is put under shear stress due to rotation. In this technique there are two opposite forces of rotation that causes this pressure by forcing the sample in two different directions. This technique is fast and can handle large volumes. Other benefits include sterility as this can be performed all in one container and not having to use any organic solvents. DC does not need any size reduction after initial preparation, as the shear forces reduce the size of the liposomes during preparation. VPGs is the product that is initially formed, and as with the "one step" preparation technique, they can be diluted into SUV dispersions and go through characterization (Ingebrigtsen et al., 2017; Has & Sunthar, 2019).

### 1.1.3 Processing liposomes

A rather important characteristic of liposomes is their size, as it affects both their *in vivo* and *in vitro* properties. The size will affect the drug load of the liposomes, which determines the dose needed for therapeutic effect. Size also affects aggregation and sedimentation, and thereby the stability of the liposomal formulation. Blood distribution, the circulation time and bioavailability are also determined by the size of liposomes (Eroğlu & İbrahim, 2020).

Vesicle size directly affects how fast the body eliminates foreign particles. Liposomes larger than 200 nm are quickly recognized and eliminated by opsonization of the RES, while nanoparticles smaller than 70 nm are able to enter and accumulate in the liver, thereby being removed from circulation. As such it can be argued that the size of liposomes in a liposomal formulation should be between 70 nm and 200 nm (Hupfeld et al., 2006; Sercombe et al., 2015).

An advantage of liposomal size is that it is adjustable as there are several ways to reduce the size, such as extrusion and sonication, some of the more used methods. The downside with these methods is that only small volumes of liposomes, as well formulations with low lipid content, can be used at a time (Has & Sunthar, 2019). To make larger volumes of smaller

liposomes, a high pressure homogenizer can be used, utilizing the microfluidizer (Schuh et al., 2018).

#### 1.1.3.1 Sonication

Sonication is a highly used method for size reduction of liposomes (Akbarzadeh et al., 2013). There are two types of sonication methods; probe sonication and bath sonication. A probe sonicator comes in direct contact with the formulation, something that can cause contaminations due to the formulation being in an open environment. The sonicator probe exposes the formulation to high amounts of energy which causes it to heat up. This energy consists of waves of pressure, which breaks apart various substances. To counteract this, an ice bath is usually placed under or around the formulation container. When using a bath sonicator, the container is submerged in water that is then exposed to sonication waves. This method gives much better temperature control in comparison to probe sonication. This allows for sterile processing, however the efficacy of the size reduction is generally not satisfying for gaining ideal size for drug delivery. Common limitation with both of these techniques is that it can give a broad vesicle size distribution. Another limitation is that sonication machines are only really used for lab scale production, and poorly suited for industrial manufacturing (Akbarzadeh et al., 2013; Has & Sunthar, 2019).

#### 1.1.3.2 Extrusion

There are several types of extrusion, however the membrane extrusion is common for lab production and is a highly used method for liposome size reduction. This method uses a nanoporous membrane, which breaks apart larger MLVs in to smaller MLVs or ULVs. It does this by forcing the larger vesicles through the membrane, which has smaller pores then the size of the vesicle. Compared to sonication, extrusion while more time consuming, produces liposomes of a narrower size distribution and gives reproducible homogeneous systems. However, in addition to being lab scale, membrane extrusion has the downside of product loss due to lipid being lost in the membrane (Guo et al., 2018).

#### 1.1.3.3 Microfluidizer

For size reduction of liposomes, a microfluidizer works by exposing the liposomal suspension to cycles of homogeneous pressure and using this to forcefully collide the suspension in a high

impact zone. Because of high shear impact forces, large liposomes are broken into several smaller ones. The impact zone will be at the end of the microfluidizers interaction chamber, which is "Y" shaped (Figure 3). This technology can perform pressure cycles of up to 30 000 psi. By adjusting the pressure itself and the number of passes through the chamber, it is possible to tailor the outcome of liposomal size (Ganesan et al., 2018; Schuh et al., 2018).

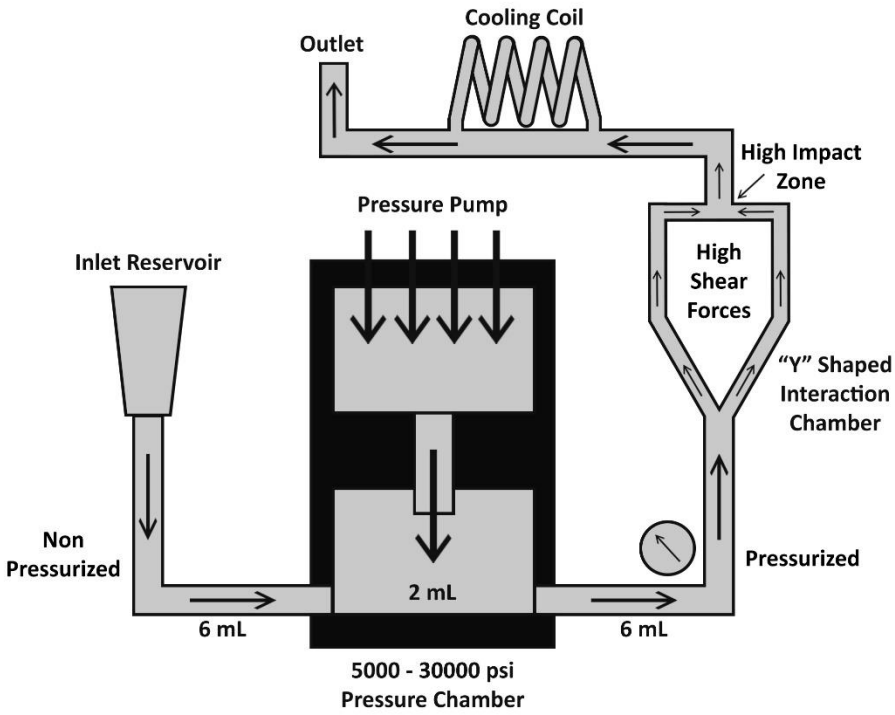


***Figure 3:*** *Schematic overview of the basic principle of a microfluidizer. Figure adapted from (Khan et al., 2014; Ganesan et al., 2018).*

How many passes and what level of pressure is needed to achieve desired size, is different for each formulation and the resulting system may not necessarily be homogeneous. There are reports that while the microfluidizer could produce SUVs down to 20 nm, it only did so in polydisperse systems. This means that a microfluidizer can prepare both MLVs, LUVs and SUVs depending on the pressure and number of passes. As such a wide variety of sizes are achievable with a microfluidizer, and making large quantities of liposomes within the desirable size rage of 70 - 200 nm is well within the size scope of this machine (Ganesan et al., 2018; Schuh et al., 2018).

### 1.1.4 Characterization of liposomes

After the third stage of liposomal preparation, the liposomes go through processes of characterization. Here the size, surface charge (zeta-potential) and other characteristics such as lamellarity, encapsulation efficiency and membrane rigidity are determined (Kanasova & Nesmerak, 2017).

For size determination there are several different methods. One of them is Dynamic Light Scattering (DLS) also known as Photon Correlation Spectroscopy (PCS). DLS uses the intensity of scattered light by liposomes under Brownian motion at a given angle to measure the size distribution. Brownian motion describes the movement of dispersed vesicles or particles which varies based on their size. By aiming a light at a dispersion, this movement will scatter it and reflect varying intensity of light. The fluctuations in the intensity over time allows estimation of the distribution of the vesicle diameter (Hupfeld et al., 2006; Bian et al., 2016). Likewise, the surface charge of liposomes can be estimated by the spectroscopic measurement of the zeta-potential. Electrophoretic mobility and DLS are used to assess the distribution of vesicle surface charge (Ternullo et al., 2019). DLS has several advantages as it is easy, accurate and can be used without disrupting the natural environment of the sample. It is however, not the best at determining the size of very small vesicles that are only several nm in diameter, or highly polydisperse systems. For this kind of size measuring, other techniques should be taken into consideration (Hupfeld et al., 2006; Kanasova & Nesmerak, 2017).

Electron microscopy is also a much utilized technique to determine the size of individual liposomes. Moreover, this technique can also be used to visualize the liposome and determine their lamellarity and morphology. Electron microscopy uses electrons to illuminate a sample instead of photons like in a light microscope. Because of this it manages to get high resolution images down to the nm scale. These images can visually reveal the size, structure and lamellarity of the illuminated sample. Some drawbacks of this technique include the tedious, time consuming and complicated sample preparation, as well as potential vesical shrinkage and/or shape distortion. Because of this, techniques like DLS are much more utilized as routine measurements (Kanasova & Nesmerak, 2017).

Other ways to determine lamellarity is through Phosphorus Nuclear Magnetic Resonance ($^{31}$P NMR) with the addition of manganese ions ($Mn^{2+}$). The lamellarity can be calculated by comparing the $^{31}$P resonance signal from before and after addition of $Mn^{2+}$. This is because

$Mn^{2+}$ can react with negatively charged phosphate groups on the liposomes phospholipids, and this will make the second signal lower than the first as there will be less phosphate. While this technique can be accurate, a disadvantage is that there is no differentiation of whether the ions were evenly distributed or not. This can lead to potential false readings (Kanasova & Nesmerak, 2017).

Another characterization that is performed on processed liposomes is their encapsulation efficiency, which represents the amount of drug that is encapsulated in the liposome. This measurement can be an important factor in the making of a liposome formulation, as the amount of drug present will help in determining the therapeutic dose. The encapsulation efficiency is usually measured in two steps. First the excess un-encapsulated drug is removed using different forms of centrifugation or dialysis. Then this sample is measured using a variety of different techniques like spectroscopy or chromatography, to determine the remaining drug. From these measurements, the percentage of encapsulated drug can be calculated different ways. A rather common way includes:

% encapsulation efficiency = initial drug-drug loss/initial drug (Kanasova & Nesmerak, 2017).

### 1.1.5 Cellular uptake of liposomes

Liposomes are known to be able to deliver encapsulated drug/compound to cells. There are several mechanisms known that the liposomes utilizes for delivery of these molecules and for internalization of the liposomes. These include fusion with the cell membrane, adsorption, lipid transfer and endocytosis (Figure 4, p. 13). Fusion while rare, happens when and if the liposome is in close contact with the cell membrane, causing the membrane of the liposome to merge with the lipids in the membrane. This allows the payload to enter the cell cytosol directly. Fusion is said to happen more for cationic liposomes, however this could potentially alter the cells own surface potential. Adsorption will only happen if the repellent forces of e.g. surface charges between the liposome and the cell are overcome by other attractive forces such as the formation of van der Waal or hydrogen bonds. When this happens the liposome is pulled close to the cell, allowing for the transfer of components. With lipid transfer, the lipids in the liposome exchange lipids and other membrane components with the cell membrane. In endocytosis, the entire liposome in engulfed into the cell (Rodrigues et al., 2019; Gomez & Hosseinidoust, 2020).

These first three mechanisms exhibit low efficacy in delivering the molecules to the cell. On the other hand, endocytosis has higher efficacy and is also the most common way for liposomes to interact with cells. There are several different ways of achieving endocytosis, including macropinocytosis, receptor mediated endocytosis via clathrin-mediated endocytosis or caveolae-mediated endocytosis, as well as clathrin-independent and caveolae-independent endocytosis. The absorbed liposomes end up being degraded and broken down by the endosomal-lysosomal system. This degradation allows for the release of molecules from the liposome to the cytosol, however sometimes the liposomes are degraded along with their payload (Daraee et al., 2016; Rodrigues et al., 2019).

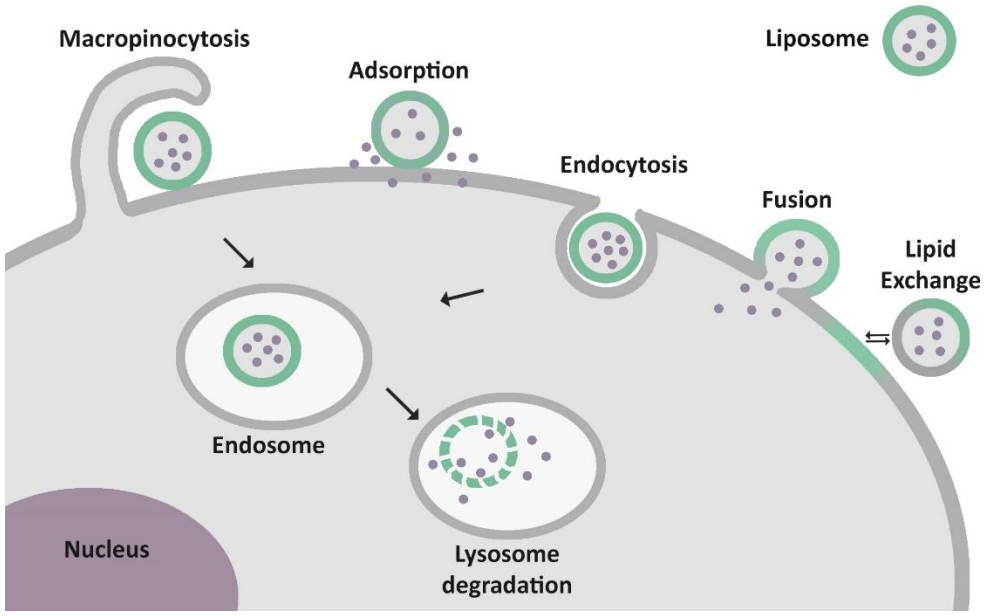


***Figure 4:*** *Different mechanisms of liposome cell interaction and internalization. Figure adapted from (Agarwal et al., 2016; Rodrigues et al., 2019).*

### 1.1.6 Toxicity of liposomes

Since liposomes are made from non-toxic phospholipids, they are considered less toxic than other materials such as synthetic polymers or metals. This is likely due to their potential to mimic naturally occurring cell-membranes (Bozzuto & Molinari, 2015). This, however does not mean that liposomes do not have potential for toxicity. If the lipids are cationic they can be toxic as positively charged liposomes can lead to cell shrinking, less mitosis or other detrimental effects due to the disruption of the cell charge and surface proteins (Wilczewska et al., 2012; Dos et al., 2018).

Remains from organic solvents that were used during the preparation phase, can also be of concern, as these are considered toxic (Danaei et al., 2018). There are also other potential contaminants to worry about, such as metal ions, as these too can potentially cause toxicity. This kind of contamination can come from sonication probes or machines like a microfluidizer (Wagner & Uhl, 2010; Danaei et al., 2018). Other potential toxicity issues for liposomes are correlated to their size. Liposomes larger than 200 nm (LUVs and MLVs) are opsonized and detected by the RES, such as the liver, spleen and lymph, which can potentially cause an unwanted immunoreaction (Hua & Wu, 2013; Sercombe et al., 2015).

However, the toxicity of any nanocarrier including liposomes, depends on the target it reaches. Poor distribution can e.g. lead to the carrier not reaching the intended target, but rather another one. This can lead to unpredictable effects that can be toxic, not only from the nanocarrier, but also from the active ingredient they carry. For this reason, evaluating the targeting efficiency of a carrier as well as the drug beforehand is vital for a formulation development (Wilczewska et al., 2012).

## 1.2 Fluorescence as a tool to visualize liposomes

Fluorescence is the emission of colored light from a molecule that has absorbed light. Fluorescent emission is almost always within the visible spectrum of light, because of this the emitted light is colored and visible to the human eye. This phenomena can be used to produce an image via fluorescent imaging, as colored light will stand out against an otherwise dark background. Fluorescent imaging of a sample is possible by labeling/staining it with a fluorescent compound and then combine that with a suitable imaging instrument (Lichtman & Conchello, 2005; Boreham et al., 2017).

Preparing a fluorescent formulation is usually done by adding fluorophores, fluorochromes or fluorescent dyes, as these are molecules capable of producing fluorescent light. Adding these kind of molecules in an early stage of liposome preparation will allow the formation of fluorescently labeled liposomes, which can be traced with the help of fluorescence-based imaging techniques (Boreham et al., 2017; Ali et al., 2019).

### 1.2.1 Mechanism

Fluorescence occurs when light is emitted by molecule excitation and relaxation, a process involving an electron absorbing light and then emitting light of a different wavelength. When an electron in a molecule capable of emitting florescent light absorbs light (photons) of a particular wavelength, it becomes exited. This can move the electron from its ground state into a different orbital farther away from the nucleus, giving it higher energy. This higher energy state is highly unstable and as such the electron will eventually relax back to the ground state. When this happens, the electrons can emit fluorescent light of a different wavelength than the one that made them exited. These two wavelengths of light are referred to as the excitation and emission wavelength of a fluorescent molecule. The wavelengths vary between all the different fluorescent molecules (Boreham et al., 2017).

The relaxation of the electrons happens in different phases, as described with a Jablonski diagram (Figure 5, p. 16). When an electron is exited, it moves from the ground state ($S_0$), to the exited state ($S_1$, $S_2$). In between these states there are intermediate nonstable rotation and vibration levels. The relaxation phases after entering the exited state, involves the electron moving to the closest lower stable electronic level. For the first stage this means that if the electron ends up at $S_2$ after excitation, it will try to move down to $S_1$. This is because $S_1$ has a lower electronic level than $S_2$ that is more stable than any of the intermediate levels. The electron will because of this, shift away from its original position. This process is called internal conversion (IC) and is a non-radiative relaxation, meaning it does not emit light (Lichtman & Conchello, 2005; Boreham et al., 2017).

For the second relaxation phase, the electron will move from $S_1$ and down to ground level ($S_0$). This movement happens because the electron again moves to the more stable electronic level, here from $S_1$ to $S_0$. During this process the electron emits light (photon) and as such it is called radiative relaxation. However, the wavelength of this light has changed from that of the original exiting photon due to the shift of the electron from IC. This process of relaxation and light emission is called fluorescence, and the light emitted is fluorescent (Lichtman & Conchello, 2005; Boreham et al., 2017).

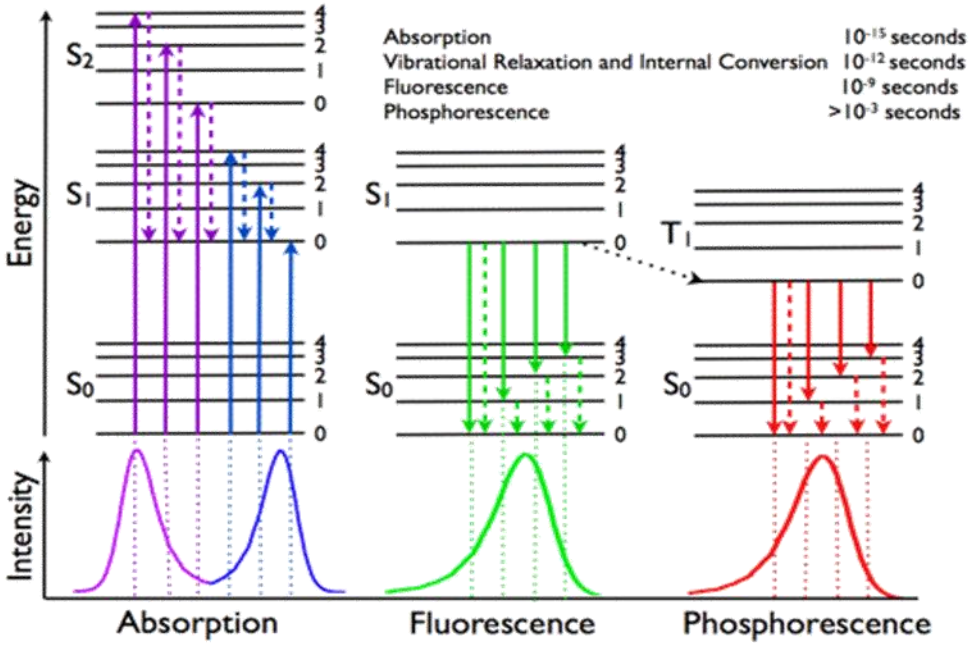


***Figure 5:*** *Jablonski diagram depicting viable energy levels and movements between possible electronic states of a fluorophore. (Admin, 2014).*

There is also a third step, where the electron instead of moving from $S_1$ to $S_0$ immediately, moves from $S_1$ to $T_1$. It does this because $T_1$ has a lower stable electronic level than $S_1$. The electron can then move to $S_0$ or back to $S_1$. This process is called inter system crossing (ISC). The transition from S to T and vice versa is much slower than the other potential movements of the electron. When the electron is at $T_1$, it can move to $S_0$ with either a radiative or non-radiative relaxation. If the process is a radiative one, it is called phosphorescence, and it is a delayed release of the exiting photon. If the electron moves back to $S_1$ and then to $S_0$ the process is called delayed fluorescence (Boreham et al., 2017).

### 1.2.2 Fluorescent spectroscopy

Fluorescent spectroscopy is able to analyze the fluorescence of a sample. It can do this by first exiting the sample with light of a specific wavelength. The machine has two filters, an excitation and emission monochromator. These filters filter the excitation and emission wavelength so only the excitation hits the sample and only the emission the detector. The amount of fluorescence signal from a sample can directly be correlated to a sample concentration, and as such is widely used to determine concentration of solutions and similar. Due to this it can also

be used to determine the concentration of a fluorescent molecule entrapped in a liposome (Croneya et al., 2001; Boreham et al., 2017).

### 1.2.3 Fluorescent imaging

Fluorescent microscopy is a powerful tool that can be very useful in drug delivery to locate and visualize the distribution pattern of different fluorescent carriers. Since fluorophores each emit light with a specific wavelength, they can be traced through their emission by detection of their wavelength. Detecting only the returning light (the emission) can be done by filtering out any other wavelengths. Because of this mechanism, fluorescent microscopy uses reflected light instead of transmitted light to illuminate an image (Lichtman & Conchello, 2005).

In a fluorescent microscope, the exiting light needs to be separated from the rest of the beam before illuminating the sample. This requires a beam splitter, known as a dichroic mirror coupled with a filter that can separate the specific excitation wavelength needed to excite the electrons in the sample. This dichroic mirror and filter are often build together as a cube. The light beam (e.g. a laser) is sent through the filtered dichroic mirror, separating out the excitation wavelength. This is then reflected down through an objective onto the sample, causing it to become exited and give off fluorescent light. The fluorescent emission is then reflected back up through the dichroic mirror allowing the visualization of the colored fluorescent sample against a dark background. This makes for good images of otherwise colorless samples (Lichtman & Conchello, 2005).

### 1.2.4 Flow cytometry and cell Imaging

Flow cytometry is widely used to quantify cell data and is a technique that works by separating, counting and analyzing cells. The separation of cells happens in a flow chamber (also known as a flow cell). In the flow chamber, there is a constant controlled fluid stream called the sheath fluid. This fluid moves and aligns the cells from a concentrated cell suspension to a single-cell stream, this alignment is called hydrodynamic focusing. The cells, now one by one, pass through a laser beam. When the light emitted by the laser hits a cell, it is scattered into multiple directions due to the photons colliding and interacting with the cell. This scattering is grouped into two different categories according to the position of the detector: forward scatter (FSC) and side scatter (SSC) (Figure 6, p. 18) (Pereira et al., 2018; Park et al., 2020).

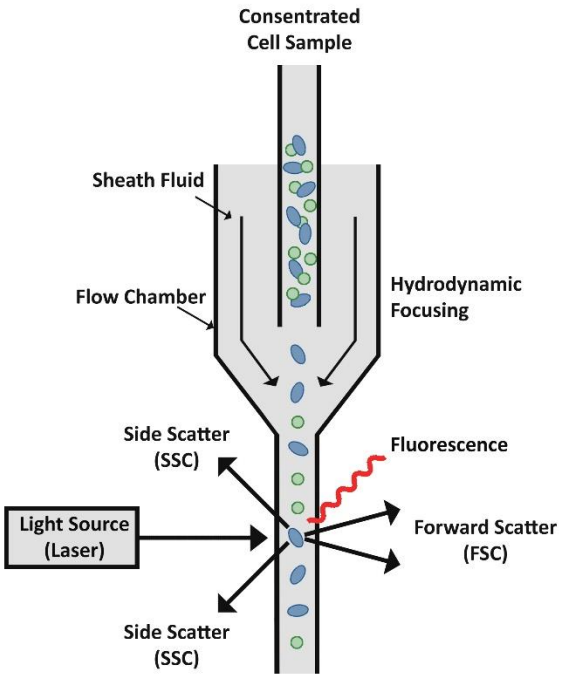


***Figure 6:*** *Schematic overview of the basic principles of flow cytometry. Figure adapted from (Kanasova & Nesmerak, 2017; Pereira et al., 2018).*

Flow Cytometry is often coupled with a variety of different technologies. When flow cytometry technology is used with a cell sorter, it enables Fluorescence Activated Cell Sorting (FACS). FACS accelerates the separation of cells and the liquid stream of cells are separated into droplets. These droplets can then be sorted and collected based on their charge. FACS in the addition to measuring and analyzing FSC and SSC, also have the detectors needed to register fluorescence should electrons in the cell become exited due to the laser. These fluorescence detectors have the ability to filter out any unwanted wavelengths. The intensity of the measured light and fluorescence is then converted into electrical signals (voltage) that can be processed by a computer. The generated data can be used to perform an analysis of multiple parameters of the cell sample, like size or inner cell complexity (Pereira et al., 2018).

By combining flow cytometry and fluorescent microscopy, Imaging Flow Cytometry (IFC) is enabled. IFC technology enables the collection of single cell information, while also capturing fluorescent images of single cells. Several advantages of IFC include their high resolution imaging ability, their fluorescence sensitivity and high speed processing. The high resolution images enables the analyzing of potential changes in morphology and cell functions like phagocytosis (Han et al., 2016; Park et al., 2020). One technology incorporating IFC is called Image Stream X (ISX) (Chia et al., 2017).

### 1.2.5 Fluorescent liposomes and their use

By labeling liposomes with a fluorescent substance, it is possible theoretically, to locate and visualize where our liposomes are with fluorescent imaging. Fluorescent liposomes are therefore used for the real time visualization of liposomal organ accumulation and distribution. This is beneficial as it provides understanding of the drug delivery process as well as predicting therapeutic potential of the liposomes. Fluorescent liposomes are also utilized within theranostics (treatment and diagnosis). This means that these liposomes contain one diagnosing element, like an imaging molecule (e.g. a fluorophore) and a drug for treatment (Lammers et al., 2011). It is however, important to remember that it is the fluorophore that is being imaged, and not necessarily the liposome. Liposomes leak their content (Monteiro et al., 2014; Münter et al., 2018) so the image might be showing the distribution and accumulation of the fluorescence instead of the liposome and/or drug. If this is the case, the visualization might give incorrect analyses as the analyzed distribution then belongs to the fluorescent compound and not the formulation (Snipstad et al., 2017).

### 1.2.6 Rhodamine B

Rhodamine B is a bright red fluorescent dye often used for fluorescent imaging through staining (Sigma-Aldrich, 2019) (Figure 7). It is highly soluble in both water and alcohols, but has a partition coefficient (Log P) of 1.95 in octanol vs. water. Due to this, in a liposomal formulation, rhodamine enables detection of the bilayer (Martina et al., 2007).

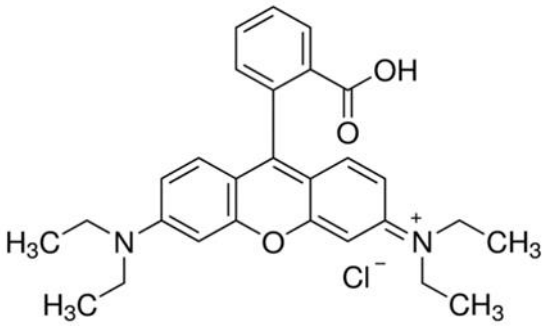


***Figure 7:*** *Chemical structure of rhodamine B (Sigma-Aldrich, 2019)*

### 1.2.7 Curcumin

Curcumin is derived from the rhizome of the plant *Curcuma longa* (turmeric). The molecule is a yellow fluorescent pharmaceutical active ingredient that has many different desirable biological activities and can be seen as an active substance. It is an antioxidant, anti-inflammatory among many other properties and is often labeled a chemo-preventive (Bansal et al., 2011; Mahmud et al., 2016). Curcumin is a highly lipophilic compound with poor aqueous solubility (Figure 8), and a consequence of this has poor bioavailability. Due to these characteristics the use of curcumin in medicine has been impeded, as it is very difficult to make a pharmaceutical formulation containing curcumin. Drug delivery of this drug is therefore important. Liposomes as well as other nano-formulations have shown to be able to overcome these issues (Mahmud et al., 2016).

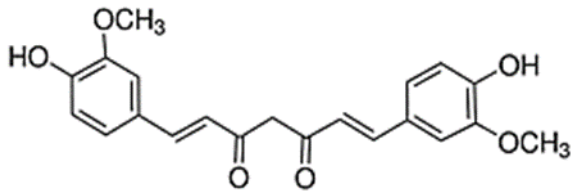


***Figure 8**: Chemical structure of curcumin (Sigma-Aldrich, 2019).*

According to the PubMed database, National Institutes of Health, there has been more than 390 publications featuring curcumin and liposomes published since 1987. These publications feature benefits of liposomal curcumin. Liposomes among other things enhances curcumin bioactivity such as anti-inflammatory activity and anticancer properties (Mahmud et al., 2016). A benefit of curcumin is that it also has very low cytotoxicity, especially when compared with e.g. other chemo-preventatives (Mahmud et al., 2016). Also due to its solubility and fluorescent characteristic, curcumin can help trace the liposomal bilayer via fluorescent imaging techniques (Kunwar et al., 2006).

For its pharmacological activity, curcumin exhibits a variety of effects on signaling pathways in the body. Mostly through the inhibition of intracellular transcription factors and secondary messengers. Curcumin has been documented to cause apoptosis in oncogenic cells and prevents carcinogenesis through inhibition of Cytochrome P450 enzyme–mediated bio activation of environmental carcinogens (Bansal et al., 2011). For the anti-inflammatory activity, curcumin is known to suppress nuclear transcription factors that helps increase inflammation, such as NF-

κB, which is responsible for TNF-α activation, a major inflammatory mediator. Curcumin can also inhibit the nitric oxide (NO) production from inflamed immune cells (Prasad et al., 2014).

# 2 AIM of the study

The aim of this thesis was to optimize liposomes prepared by microfluidization in respect to their cellular fate followed by imaging. For this purpose two different fluorescently labeled liposome dispersions were optimized and compared to assure that the processing is reproducible, able to manufacture liposomes with desired characteristics. Since the aim of the prepared liposomes was imaging their cellular uptake, the fluorophores were selected to be preferably located within the bilayers.

It was hypothesized that several passes of microfluidization was needed for liposomes to achieve the preferable size of around 100 nm (SUV). Therefore the sub-aims of the project were:

- To identify the preferential processing attributes of a microfluidizer
- To assure the fluorophores location in the bilayer with minimal loss of fluorophore during processing
- To confirm that curcumin liposomes remain biologically active after microfluidization
- To image the cellular uptake of microfluidized liposomes

Finally, the stability of microfluidized liposomes was evaluated

# 3 Materials and Methods

## 3.1 Materials

Soy phosphatidylcholine (Lipoid S100) was kindly provided by Lipoid GmhH (Ludwigshafen, Germany). 1,2-distearoyl-sn-glycero-3-phosphoethanolamine-N-[methoxy(polyethyleneglycol)-2000] (ammonium salt) (DSPE-PEG) was purchased from Avanti Polar Lipids Inc., (Alabama, USA). Rhodamine B, curcumin (FLUKA curcumin purum: ≥95.0%), Dimethyl sulfoxide (DMSO), ethanol, methanol (Chromasolv®), RPMI-1640 cell culture medium, Dulbecco's phosphate buffer, fetal bovine serum (FBS), penicillin and streptomycin solution and lipopolysaccharide (LPS) were purchased from Sigma Aldrich, (Merck KGaA, Darmstadt, Germany).

## 3.2 Preparation of liposomes

Lipoid S100 was used for all the different types of liposomes prepared. The liposomes were prepared using the film method, thin film hydration utilizing a Büchi Rotavapor R-124 with vacuum pump V-700 (Büchi Labortechnik, Flawil, Switzerland). A round bottom flask of 100 mL was used each time. The organic solvent used was methanol (MeOH). The evaporation was performed with constant temperature of 45 °C, a starting rotation of 100 rpm, which was adjusted up to 120 rpm after evaporation. During this process the pressure was dropped down to 60 mBar. Due to the high lipid content, the continuous pressure reduction was performed slowly and steadily until evaporation was noticed. The system was then left on this pressure and rotation until the film appeared dry before further lowering the pressure to the 60 mBar. This took approximately 30 to 60 minutes, and was done to reduce the chance of the lipid mixture boiling. After reaching 60 mBar the flask was left on the rotavapor for an hour. This was done to remove any potential remaining traces of solvent.

After the evaporation, a lipid film was developed on the inside of the flask. This film was then rehydrated using distilled water ($dH_2O$). Both hand mixing and a vortex was used to mix and extricate the film into suspended MLVs. These liposomes were then transferred to plastic tubes, sealed and stored in a refrigerator (4-8 ºC) for a minimum of 12 hours before processing. All the formulations are listed in detail in the Appendix (Table A1 – A5).

### 3.2.1 Preparation of empty liposomes

For the empty control liposomes, 600 mg of Lipoid S100 were weighed in a round bottom flask. This was then dissolved in approximately 10 mL of MeOH, evaporated to a thin film and then rehydrated with 22 mL $dH_2O$ as described in chapter 3.2.

#### 3.2.1.1 Preparation of PEGylated empty liposomes

The PEGylated empty liposomes were made in a similar fashion to the non-PEGylated controls. However, the PEG was introduced as already PEGylated lipids in the form of DSPE-PEG. Therefore a new amount of lipid had to be weighed out as there was now two different types. As such 5 mol% DSPE-PEG was chosen to 95 mol% Lipoid S100 (Sriwongsitanont & Ueno, 2004). It was important to keep the same molarity of the lipids from the other non-PEGylated liposomes so that they were comparable. This was calculated to be 0.111 g of DSPE-PEG and 0.570 g of S100.

The 111 mg DSPE-PEG and 570 mg S100 were weighed in a round bottom flask and dissolved in 10 mL of MeOH. This was then evaporated on a rotavapor and rehydrated with 22 mL of dH2O as described in 3.2.

### 3.2.2 Preparation of rhodamine B liposomes

For the liposomes with rhodamine B a high concentration of 10 mM was chosen according to the previous work (Ternullo et al., 2017). For 600 mg lipid and 20 mL this was 95.80 mg of rhodamine, or 4.79 mg/mL.

Here 600 mg Lipoid S100 was weighed in round bottom flasks. Then 95.8 mg rhodamine B was weighed in a weighing boat and then transferred over to the round bottom flask with the help of 10 mL MeOH. An additional 5-10 mL MeOH was added to remove any powdered rhodamine from the sides of the flask. This was then run on a rotavapor and rehydrated with 20 or 22 mL of $dH_2O$ as described in chapter 3.2 (Figure 9, p. 25).

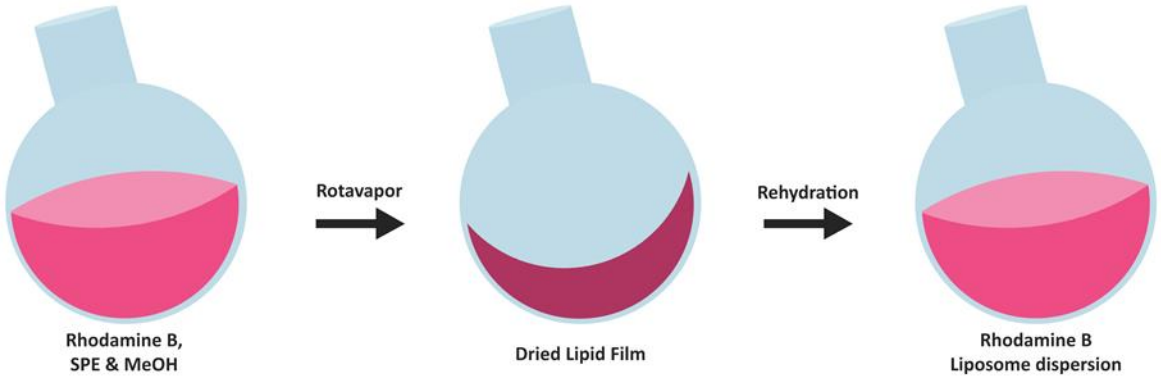


***Figure 9**: Preparation phases of rhodamine B labeled liposomes. Figure adapted from (Gharib et al., 2015).*

### 3.2.3 Preparation of curcumin liposomes

The curcumin concentration in the curcumin liposomes was chosen based on earlier work (Ternullo et al., 2019) to have a 10:1 ratio. This meant using 10 parts SPC and 1 part curcumin. These curcumin liposomes were made to have the same conditions as the rhodamine B liposomes, so that they could be comparable. This meant 600 mg SPC, and therefore 60 mg of curcumin.

For these liposomes 600 mg Lipoid S100 was weighed in a round bottom flask. Then 60 mg of curcumin was weighed in a weighing boat and then transferred to the round bottom flask with approximately 20 mL MeOH. An additional 20 mL needed to be added before the curcumin was fully dissolved, to a total of 40 mL MeOH. The solvent was then evaporated with a Rotavapor and rehydrated with 22 mL $dH_2O$ (chapter 3.2) (Figure 10).

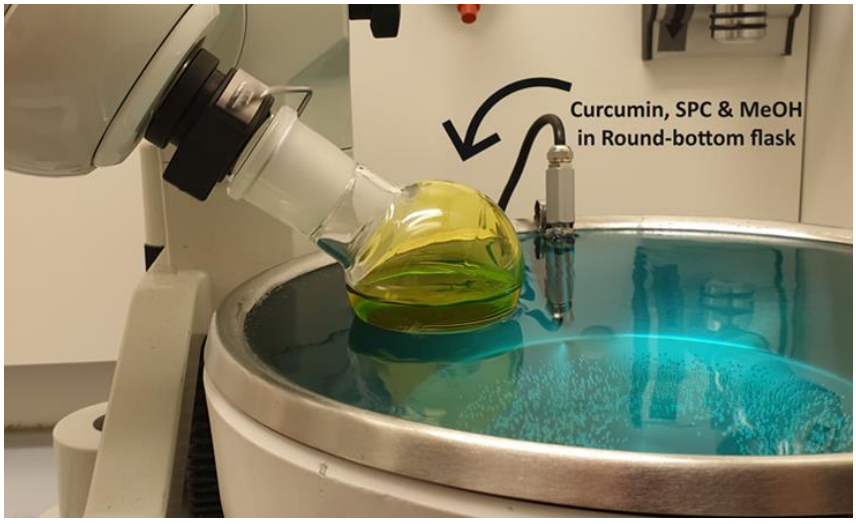


***Figure 10:** Curcumin, Lipoid S100 and MeOH in a round bottom flask, where the MeOH is being evaporated on a Rotavapor.*

#### 3.2.3.1 Preparation of PEGylated curcumin liposomes

For the PEGylated curcumin liposomes, the same lipid composition was used as the empty PEGylated controls. This meant 5 mol% DSPE-PEG and 95 mol% Lipoid S100. As this was the same amounts of SPE mol that the non-PEGylated curcumin liposomes had, it was decided to keep the 60 mg of curcumin. This would make for the same 10:1 molar ratio, as used for the non-PEGylated curcumin liposomes.

Here 111 mg of DSPE-PEG and 570 mg lipoid S100 were measured in a round bottom flask. The 60 mg of curcumin was weighed in a weighing boat that was then transferred to the flask with approximately 20 mL of MeOH. An additional 30 mL, to a total of 50 mL, of MeOH needed to be added for the curcumin to be fully dissolved. The solvent was then evaporated with a rotavapor and rehydrated with 22 mL $dH_2O$ (chapter 3.2).

## 3.3 Processing of liposomes

The processing was mainly done with an LM20 Microfluidizer Processor (Microfluidics, Westwood, MA, USA). The minimum volume usable on this microfluidizer was 18 mL, which is equal to 3 cycles. The pressure on the microfluidizer was set at 10 000 psi to begin with. This was chosen due to this pressure having been reported to make liposomes of an adequate size and vesicle dispersity (Schuh et al., 2018). Due to processing with a microfluidizer, the volume chosen for the rehydration increased from the original 20 to 22 mL because of a cycle calculation on the microfluidizer. One cycle is approximately 6 mL, and the first cycle of our sample insures a 2 mL dilution (Figure 11, p. 27). To process the suspension while accounting for this 2 mL dilution, 22 mL was used so that with the dilution we had 24 mL total, which is 4 cycles exactly to 1 pass.

The microfluidizer was prewashed with 70 % MeOH. Then before adding the MLV dispersions the MeOH was removed and exchanged with dH2O. There were four cycles to one pass, however the first six cycles were collected. The first cycle consisted of mostly colorless dH2O, and were considered a control for where the dispersion was in the system. The next four cycles were collected as the processed dispersion. The sixth was collected as a control for the percent loss of components. After this the microfluidizer was washed with 70 % MeOH. Due to the adherence of the rhodamine, the machine needed to be washed again with 70 % MeOH after approximately 24 hours.

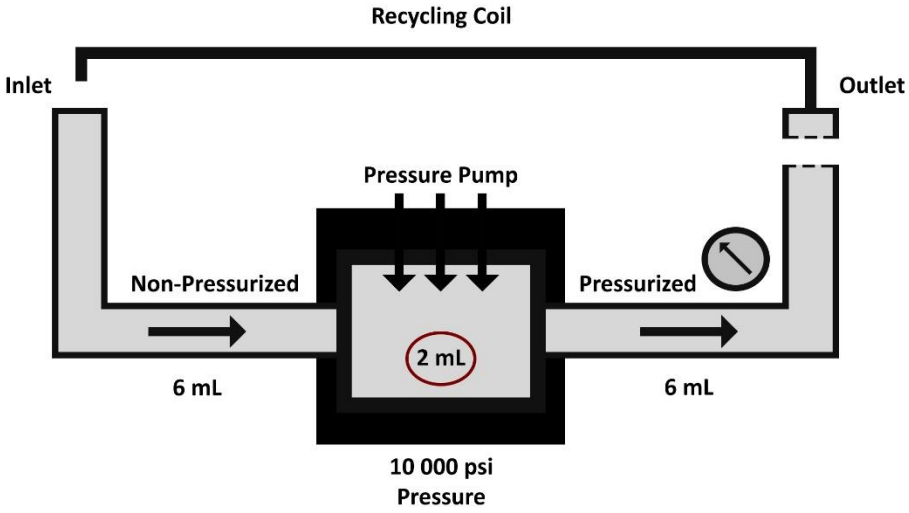


***Figure 11:*** *Overview of the volume accounted for in the inlet and outlet of the microfluidizer. Adapted from (Khan et al., 2014; Ganesan et al., 2018).*

The liposomes were mostly microfluidized at 10 000 psi with, passes varying from one to five. The empty control liposomes were passed once at 10 000 psi, with the exception of the one PEGylated control dispersion that were passed once at 10 000 psi, and then reprocessed for a second pass on 15 000 psi (Table 1).

The rhodamine liposomes were passed one to five times on 10 000 psi. Five separate dispersions were processed directly, where the dispersions were after one pass added back into the inlet reservoir with the help of the recycling coil (Figure 11) and passed again without collection until it had been passed for the intended amount of passes (one-five) (Table 1). The sixth rhodamine dispersion was first passed once without recycling, then after 24 hours characterized and processed again until it reached five passes (five days total). By processing them this way, there ended up being 2 dispersions of each of the five passes, with one being passed directly, and the other with a 24 hour separation in between passes (Table 1).

The curcumin liposomes were passed once at 10 000 PSI. The first two PEGylated curcumin liposomes were passed once and then reprocessed for a second pass. One at the same pressure and another at 15 000 PSI. It was after the results of this decided to sonicate the third dispersion first for 15 seconds then centrifuge it at 5000 G for seven minutes to get rid of free unentrapped curcumin. After this the third PEGylated curcumin dispersion was processed on the microfluidizer for one pass on 10 000 PSI (Table 1).

***Table 1:*** **Overview of the processed liposomes, amount of passes on which pressure**

| Processed liposomes | | | | |
|---|---|---|---|---|
| Formulation | Batch | Total passes on microfluidizer | Processing method* | Pressure [psi] |
| Empty conventional liposomes | 1 | 1 | Direct | 10 000 |
| | 2 | 1 | Direct | 10 000 |
| Empty PEGylated liposomes | 1 | 1 | Sequential | 10 000 |
| | | 2 | | 15 000 |
| | 2 | 1 | Direct | 10 000 |
| Rhodamine liposomes | 4 | 5 | Direct | 10 000 |
| | 5 | 1 | Sequential | 10 000 |
| | | 2 | | 10 000 |
| | | 3 | | 10 000 |
| | | 4 | | 10 000 |
| | | 5 | | 10 000 |
| | 6 | 1 | Direct | 10 000 |
| | 7 | 2 | Direct | 10 000 |
| | 8 | 3 | Direct | 10 000 |
| | 9 | 4 | Direct | 10 000 |
| Curcumin liposomes | 1 | 1 | Direct | 10 000 |
| | 2 | 1 | Direct | 10 000 |
| | 3 | 1 | Direct | 10 000 |
| PEGylated curcumin liposomes | 1 | 1 | Sequential | 10 000 |
| | | 2 | | 10 000 |
| | 2 | 1 | Sequential | 10 000 |
| | | 2 | | 15 000 |
| | 3 | 1 | Direct | 10 000 |

*Direct = Passed without pause between passes utilizing recycling coil
Sequential = Passed with a 24 hour gap between passes

## 3.4 Removal of unentrapped fluorophore

The rhodamine dispersions were dialyzed to remove any unentrapped rhodamine. The dialysis was performed using 2 mL of liposomal dispersion in a dialysis bag (membrane Mw cut off 12,000–14,000 Da, Medicell International Ltd, London, UK) submerged in 500 mL of dH2O at room temperature. The dialysis was performed for 4 hours exactly before the dialyzed suspension was collected and the dialysis medium sampled. These were then stored in a fridge and used for further characterization.

For the curcumin formulations, centrifugation was used to remove any free unentrapped curcumin. The centrifugation was done with a bench centrifuge at 3000 G for 10 minutes each. The supernatant was then removed and transferred to new Eppendorf tubes. After removing the unentrapped fluorophore, the liposomal formulations were characterized for size, zeta-potential and entrapment efficiency.

## 3.5 Characterization of liposomes

### 3.5.1 Size and zeta-potential determination

The measurements were done with liposomal dispersions left to stay at room temperature (23-25 ºC) for approximately 30 min. DLS was the technique used to determine the vesicles size, polydispersity and zeta-potential. The measurements were mostly done with a Zetasizer nano series SZ (Zetasizer software version 7.11, Malvern instruments, Oxford, UK). The setting used a sample temperature of 25 ℃, 90 s or 180 s equilibration time based on the type of measurement (size and zeta respectively), and all runs were performed in triplicates.

For the size and zeta-potential characterization normal plastic cuvettes were used to measure size and folded capillary cells (Zeta-cells, DTS 1070) were used for the zeta-potential. The cuvettes and zeta-cells were washed before and after use with 96% ethanol (EtOH) and dried before the sample preparation. The only exception was with the rhodamine liposomes, as here the washing was executed with MeOH instead due to the staining ability of rhodamine B. The sample preparation consisted of a dilution of the sample with filtered tap-water. The dilution varied for the different liposomes. The filter used to filter the water was a sterile syringe filter with a 200 nm pore size.

After drying and before use the cuvettes was washed with the filtered water to remove any traces of solvent, and then filled with the diluted sample. Any potential air bubbles were removed mechanically.

### 3.5.2 Entrapment efficiency

The entrapment efficiency of both rhodamine B and curcumin were measured using fluorescent spectroscopy (Spark Multimode Microplate Reader, Tecan, Männendorf, Switzerland). Before the samples could be measured, standard-curves of both fluorophores were made. The rhodamine standard-curve was made using a stock consisting of 1.0 mg rhodamine B and 100 mL 50% (v/v) EtOH. The curcumin stock was prepared with a stock consisting of 1.0 mg curcumin and 100 mL 80% (v/v) EtOH. 80 % EtOH had to be used to assure that curcumin was fully dissolved. The EtOH dissolves both the lipids and the fluorophores. The standard curves were made in the liner range portion (0.1 – 0.9 nm absorbance) so the concentration calculation could be accurate.

Liposomal suspensions were dissolved in their corresponding EtOH concentrations and further diluted to a measurable concentration. This dilution varied between different liposome dispersions. The measured absorbance was then used to calculate the entrapment efficiency through equation 1.

Equation 1: $$\% \text{ EE} = \frac{(\text{A}-\text{B})}{\text{A}}$$

Where A = the initial concentration, and B = the concentration measured after processing and dialysis/centrifugation.

Any absorbance of the liposomes themselves were removed and the entrapment efficiency was calculated from this.

### 3.5.3 Stability evaluation

The stability of liposomes with rhodamine B and curcumin was determined following the changes in vesicle size and zeta-potential over the course of time. These measurements were done in compliance with methods described in chapter 3.5.1. The rhodamine liposomes were measured four times over the course of 60 days. The curcumin liposomes were measured five times throughout 90 days. During these months the liposome dispersions were stored refrigerated at approximately 4 °C.

## 3.6 Determination of anti-inflammatory activity of curcumin liposomes

### 3.6.1 Cell culture

For testing the anti-inflammatory activity of curcumin in liposomes a cell culture of murine macrophages Raw 264.7 (ATCC® TIB-71TM, ATCC, Manassas, USA) was used. These cells were cultured in RPMI-1640 that was supplemented with 10 % fetal bovine serum (FBS) as well as 1 % antibiotics (penicillin and streptomycin). When the macrophages were at 90-100 % confluency, they were passaged and plated in either 6 or 24 multiwell plates. The plated macrophages were inflamed using lipopolysaccharide (LPS) in a concentration of 1 µg/mL. This method was done in compliance with (Jøraholmen et al., 2019).

### 3.6.2 Administration of curcumin

Stock solutions of both our PEGylated and conventional curcumin liposomes were made with complete medium. Other stock solutions were also prepared, namely liposome controls and curcumin controls. For the liposome controls, the conventional and PEGylated empty liposomes were prepared separately. For the curcumin control, curcumin dissolved in 30% dimethyl sulfoxide (DMSO) and $dH_2O$ was made with complete medium. Since this curcumin control contained DMSO, a curcumin free DMSO control had to be made, as such a stock solution was made with only 30% DMSO and $dH_2O$ in medium.

All stock solutions were then administered to the inflamed macrophages in the 6 or 24 multiwell plates, leaving out three for inflammation controls. The stock solution with curcumin was administered in four different concentrations of curcumin: 0.002 mg/mL, 0.02 mg/mL, 0.1 mg/mL and 0.2 mg/mL. A fifth concentration, 2.0 mg/mL, was prepared for the flow cytometry analysis. The liposome controls were also administered in four different concentrations, with a lipid concentration of 0.1 mg/mL, 1 mg/mL, 5 mg/mL and 10 mg/mL to correspond to the lipid concentration in the curcumin stocks. For the DMSO control, it was administered with the same concentrations as the DMSO with curcumin. Three wells were also treated with just $dH_2O$, at the highest corresponding concentration. These plates were then incubated overnight in 37 ºC.

### 3.6.3 NO Production

For the measurement of NO in the supernatant of the macrophages fluorescent spectroscopy was used. For this a sodium nitrate ($NaNO_2$) concentration curve was made with eight concentration points raging between 0.5 µM and 25.0 µM. Then a 1:1 ratio of Griess reagent was added to these, mixed with a vortex and measured with a Spark Multimode Microplate Reader (Tecan, Männendorf, Switzerland – Figure 12, p. 32).

When this mas made, 300 mL of supernatant was removed from each of the wells into separate tubes. Then 300 mL of Griess reagent was added into these tubes. These were then mixed well with a vortex and measured on the Spark Multimode Microplate Reader (Tecan, Männendorf, Switzerland) at 540 nm. This was then calculated into NO % with the help of the theoretical 100% of the inflamed non-treated control and the NO % measured from the treated wells.

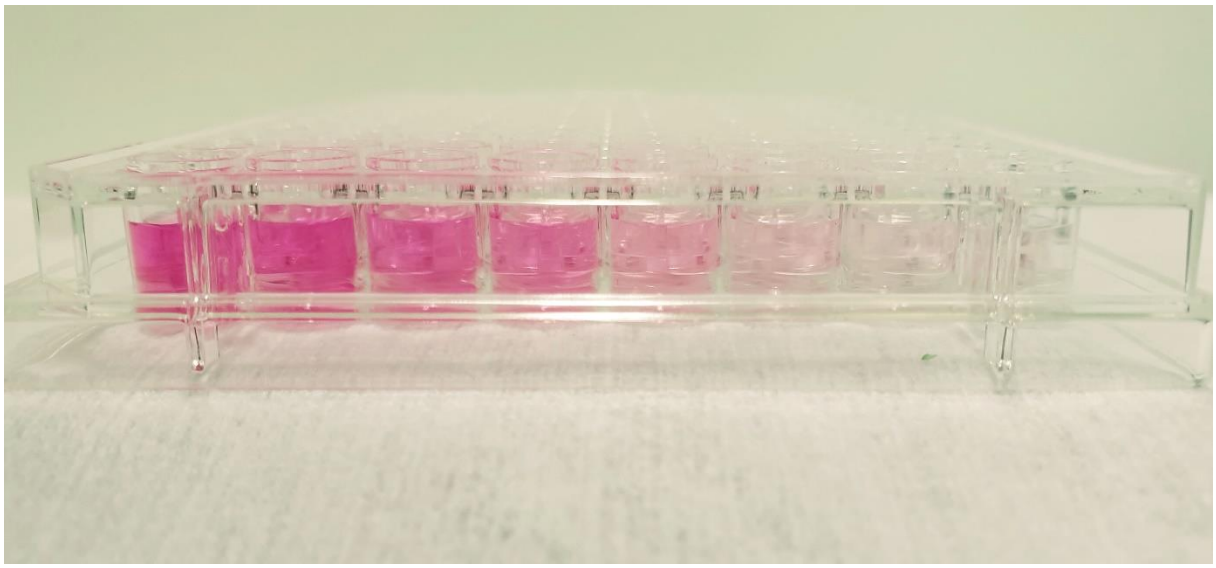

***Figure 12:*** *NaNO2 standard curve concentrations in a Spark 96 well plate. Griess reagent developes a pink colored complex with NO based on concentration.*

### 3.6.4 Flow cytometry and cell imaging

Here a FACS (FACSAriaTM with FACSDiva software version 8.0.1, BD Biosciences, San Jose, CA, USA) and IXS (ImageStreamX® with IDEAS software version 6, Amnis, Seattle, WA, USA) machine was used to analyze and image both non treated and treated cell cultures.

For these machines to operate properly, a concentrated cell sample had to be acquired. For the FACS the inflamed and treated macrophages were once at high confluency rinsed and scraped with approximately 1 mL of Dulbecco's phosphate buffer and filtered into FACS tubes. Macrophages change their shape when inflamed (Taciak et al., 2018) and this can be seen in the auto-fluorescence of the cells themselves (as verified in the calibration steps – Figure 13A, p. 33). The non-treated control of LPS-inflamed macrophages was run into the machine to set the voltage parameter in FSC and SSC. A primary gating was then selected in the FSC vs. SSC plot of events, to exclude cellular clumps and debris (Figure 13B, p. 33). Debris were excluded at a 20 000 threshold, in order to optimize the count of events inside the gate of interest (70 000). Signals from very high FSC and/or SSC were excluded as linked to cellular clumps. Then the treated cells were loaded into the machine and their FSC, SSC and fluorescence (V-500 channel) was analyzed. The setup for the flow cytometry was selected in accordance with earlier work (Bellavancea et al., 2010).

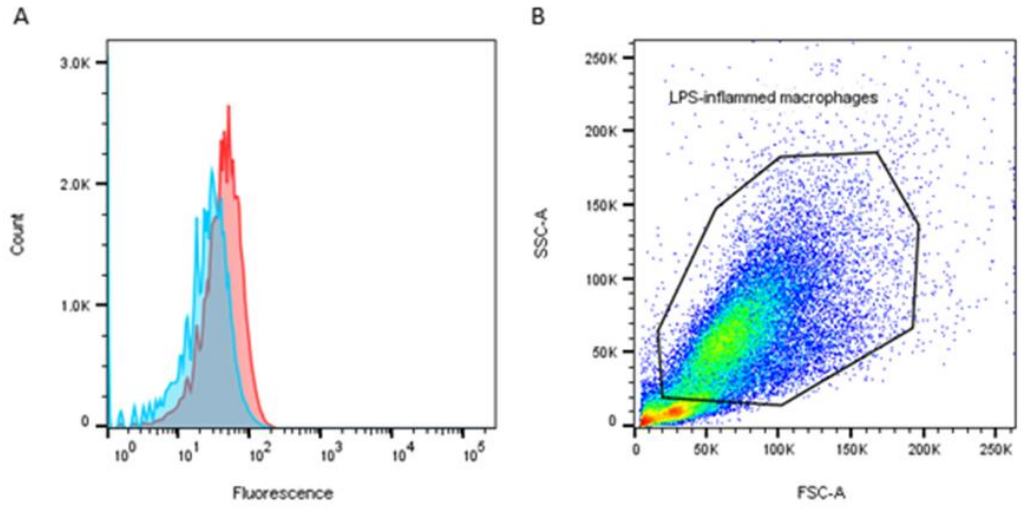


***Figure 13:*** *Flow cytometry method setup. A) Direct overlay of auto-fluorescent signal from untreated non-inflamed macrophages (blue curve, sample 1) and LPS-inflamed macrophages (red curve, sample 2). B) Scattered plot of events in forward vs. side scattering where the gate of interest for LPS-inflamed macrophages was selected.*

For the IXS, the same sample of cell suspension in buffer was concentrated by spinning them down in a bench centrifuge (1000 G for 1 min), removing the supernatant, and re-suspending the pellet. This sample was then loaded into the ISX that can read down to 12 µL samples. Here 100 images were acquired in high sensitivity of the camera and low flow. The setup for the ISX was done according to earlier work (Wayne et al., 2019).

# 4 Results and Discussion

This project was focused on the optimization of the microfluidizer in the mass production of liposomes for imaging purposes. Various characterizations of the liposomes were therefore important information, as that meant more parameters could be look screened for optimization. Labeling the liposomes with fluorophores was done to make the dispersion traceable with the help of fluorescent imaging, such as fluorescent microscopy and FACS and IFC. This however was not the only reason that fluorophores were used. Fluorophores often in addition to being fluorescent are also colored. By adding it, the liposome dispersions themselves became colored. This made it possible to visually trace them on the microfluidizer. If the product from the microfluidizer was colored, it confirmed the presence of the dispersion. Fluorescent compounds were therefore added to enable characterization through fluorescent imaging (e.g. entrapment efficiency) and for the ability to follow the microfluidizer process visually.

There were two different fluorescent compounds used, rhodamine B and curcumin. Rhodamine B is often used to trace a liposomes bilayer. It also has a distinct bright pink reddish color, and gives off red fluorescent light (Martina et al., 2007). Curcumin was, after the main optimization phase, chosen due to being fluorescent as well as a pharmacological active ingredient, exhibiting anti-inflammatory and anti-oxidative activities along with being a chemo preventative (Mahmud et al., 2016). Here the focus was on the anti-inflammatory nature of curcumin. Because of this, the anti-inflammatory activity of liposomal curcumin also had to be examined.

## 4.1 Versatility of the microfluidizer

To test the versatility of the microfluidizer, we first focused on assessing its performance within each cycle, such as size reduction outcome and entrapment efficiency. By doing this, it allowed the evaluation of the effect prolonged processing had, versus the reprocessing of an older batch. This was evaluated because being able to utilize the same batch to obtain more than one condition would significantly affect the time and material spent during the optimization phase of a new formulation.

The rhodamine formulation was prepared six times, and were passed a different amount of times for the optimization process. Five of the six dispersions were processed directly. When being passed directly, the dispersions were added back into the inlet reservoir with the help of

the recycling coil, without being collected until it had been passed for the intended amount of passes (one-five). This gave five individual dispersions that were passed one, two, three, four and five times (Table A8 – Appendix). The last dispersion was processed sequentially, one pass at a time with 24 hours in between the passes. Here the dispersion was passed once and collected, and then passed again the next day after characterization, until five passes were reached (five days total). By processing them this way, there ended up being 2 dispersions of each of the five passes, with one being passed directly, and the other with a 24 hour separation.

After the processing with the microfluidizer, the liposomes were characterized. The size, size-distribution, zeta-potential, percentage of encapsulated rhodamine and stability of the processed liposomes were tested.

### 4.1.1 Size

Since the liposome dispersions were prepared using thin film hydration, which produce MLVs, they had to go through size reduction. In this case that was mainly achieved with a microfluidizer. A pressure of 10 000 PSI was chosen to begin with due to it being reported to give vesicles of adequate size (Schuh et al., 2018). This processing seems to have given the dispersions high polydispersity, as shown with the Polydispersity Index (PDI). A high polydisperse system is not ideal, as this can negatively affect their stability (Danaei et al., 2018). The dispersions of both empty liposomes and rhodamine liposomes resulted in two main size peaks. The polydispersity of these liposomes were 0.5, which indicated that the system did not have a good uniformity of vesicles.

The empty controls that were passed once had an average of 27.38 nm (SD: 4.54 nm) for the first peak, and an average of 159.6 nm (SD: 42.45 nm) on the second peak (Table A6 – Appendix). For the rhodamine liposomes, due to the amount of passes varying between one and five, the size also varied. However the first one to four passes had comparable peaks with the first one being between 11 nm and 23 nm (SD: 1.87–5.36 nm), and the second peak between 140 nm and 164 nm (SD: 31.67– 40.46 nm). At the fifth pass, the size of the first peak was comparable to the rest, however the second peak seemed to have increased to closer to 200 nm. The PDI of these liposomes is also high, ranging from 0.3 to 0.7 (Figure 14, p. 36; Table A8 – Appendix). As expected, the PDI tends to decrease with the number of passes, but with values still above the acceptable 0.25 for homogeneous populations. The size distributions also

gradually move more towards the smaller liposomes, making these peaks gain a higher intensity (A% – Figure 14).

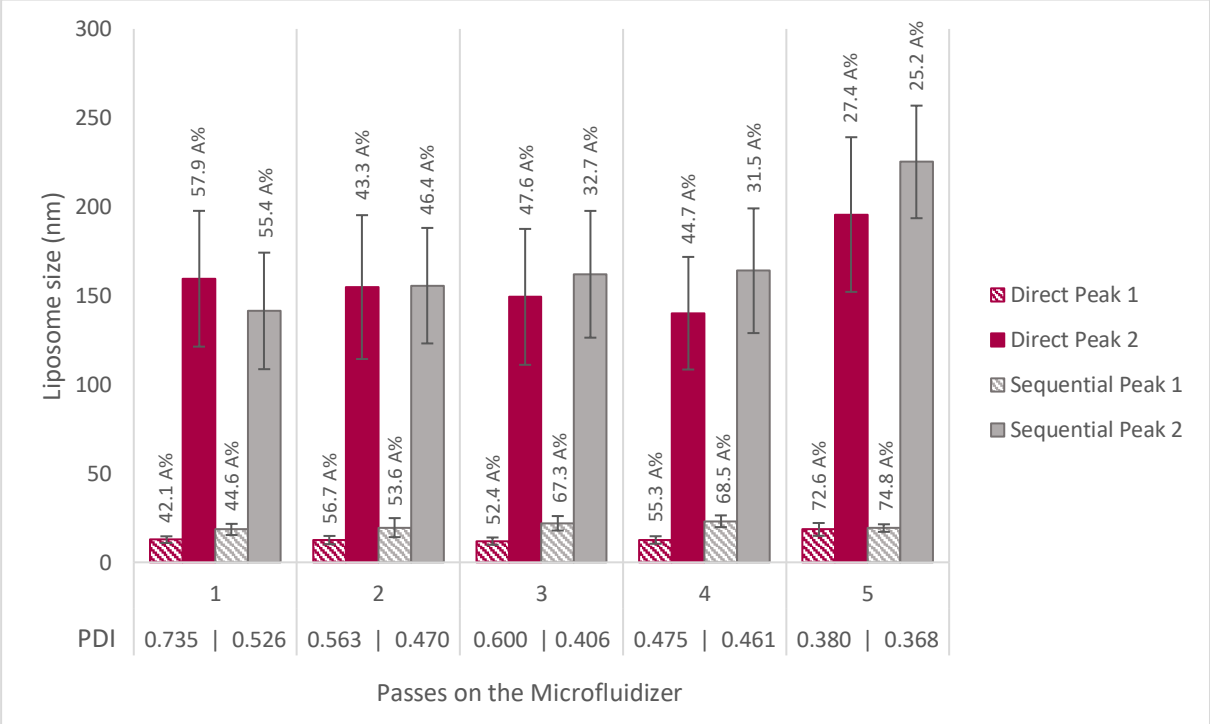


***Figure 14:*** *Mean size of both size peaks of rhodamine labeled liposomes after 1 - 5 passes on the microfluidizer. Direct = All passes were performed without interruption utilizing a recycling coil on the machine. Sequential = The characterization step was performed after each pass (repeated approx. every 24h) to obtain the most information out of the same batch. A% = the intensity of the measured size.*

From this similar size outcome, these different methods of processing seem to be comparable in vesicle size prediction. Because of this, predicting and analyzing characteristics such as size for an optimization phase is possible by reprocessing older batches. This can however use up some of the dispersion every time the characterization takes place, including the excess loss due to the reprocessing.

During the first four passes, the size does not seem to change significantly. This is probably due to the first pass being responsible for most of the lamellar reorganization and consequent size reduction. Reprocessing an additional three times other than size reduction, moved the intensity percentage (A%) in favor of the smaller liposomes (Peak 1, Figure 14). For these rhodamine-containing liposomes, the fifth pass caused a further lamellar reorganization to take place. This one however, likely did so with cohesion between the bilayers of the vesicles, ending up in larger liposomes. This means that the fifth pass here had an effect of size increase as well as on the A% of the peaks.

This method of processing liposomes showed a very quick size reduction from MLVs to LUVs and SUVs. This is beneficial as that could potentially permit processing of large volumes of usable vesicles sizes for drug delivery in a short amount of time. Evident downside for this formulation was the high polydispersity of the final dispersions. Liposomes smaller than 70 nm have shown accumulation in RES tissue, like the liver. This can be a potential for toxicity, especially if there are large quantities of smaller liposomes, like seen with the liposomes passed five times (Sercombe et al., 2015). This however, may also be exploited if the intended target is RES tissue. Accumulation of these liposomes in RES could e.g. be used to image organs such as the liver or spleen for diagnosis or treatment through fluorescent imaging.

### 4.1.2 Zeta-potential

The zetasizer when measuring zeta-potential, it takes into consideration the stabilization of charges, or the net-charge around neutral molecules and vesicles. The hydrophilic part of the phospholipids are neutral due to them having charge that counter-balance each other in zwitterionic form. If a rearrangement happens to make them uneven, it can cause a spike in the surface charge. These charges will count towards the zeta-potential, and they can also potentially interact with other charged compounds (Makino et al., 1991). Another type of charge affecting the zeta-potential can come from a pH change. It has been shown that a change in pH can have effects on the zeta-potential of liposomes (Smith et al., 2017), e.g. a high pH can give a more negative zeta-potential (Mozuraitytea et al., 2006).

For the empty liposomes, a neutral zeta-potential was expected. This is because the expected zeta-potential of liposomes consisting of phosphatidylcholine, as well as a non-charged compound, is neutral meaning virtually no charge (Matos et al., 2003; Smith et al., 2017). The measured zeta-potential was slightly above zero at an average of 0.59 mV (SD: 1.65 mV) (Table A7 – Appendix). This however is within the range of what is normally considered neutral liposomes, at a range between –10 to +10 mV. Anything outside of this area, would be considered either cationic (≥+10 mv) or anionic (≤–10 mV) (Smith et al., 2017).

A highly positive and varying zeta-potential was measured for the rhodamine B liposomes. The measurements varying between 12.00 mV and 40.60 mV (SD: 0.65–3.68 mV). The zeta-potential seems to be higher for the ones that were passed directly rather than sequentially (on the same batch), with a zeta-potential between 29.70 mV and 40.60 mV (SD: 0.65–3.68 mV).

For the sixth dispersion that was passed and characterized sequentially, the zeta-potential was slightly lower, between 12.00 mV and 24.00 mV (SD: 1.62–2.88 mV) (Figure 15; Table A9 – Appendix).

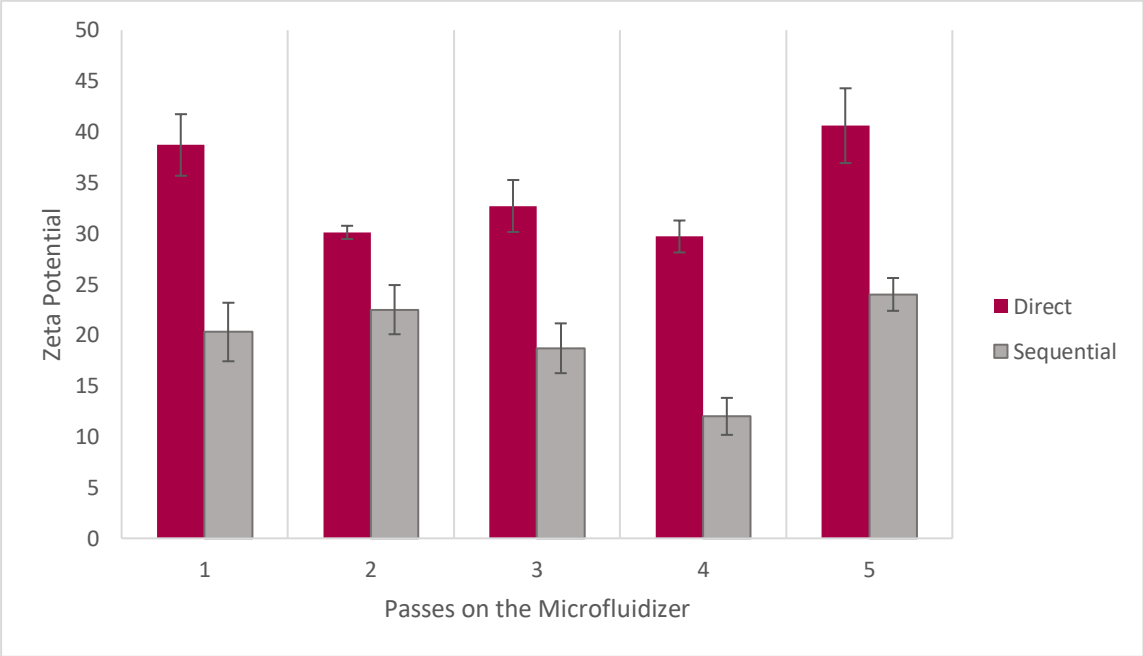


***Figure 15:*** *Zeta-potential of rhodamine labeled liposomes after 1-5 passes on a microfluidizer. Direct = 1-5 direct passes, Sequential = One pass at a time with 24 hour separation.*

These measurements point to the rhodamine liposomes having a poorly reproducible and highly unstable zeta-potential. Due to the way the zeta-potential is measured, this gives an inclination that rhodamine in this high concentration (10 mM) does not have stable interactions with the lipids in the bilayers. This can be problematic since the localization of rhodamine in the bilayer consequently cannot be confirmed. If the rhodamine was not in the bilayer, but in solution, the specificity of tracing the liposomes though fluorescent imaging was lost (Boreham et al., 2017; Münter et al., 2018).

The highly cationic values was likely caused by the rhodamine, this was also not beneficial due to highly cationic surface charge being known to be toxic due to their disruption of the cells own surface potential (Wilczewska et al., 2012). This could therefore be a problematic trait of these rhodamine labeled liposomes. Due to this, a different fluorophore was considered for the actual formulation.

### 4.1.3 Entrapment efficiency rhodamine B

The entrapment efficiency was here calculated by taking the amount of rhodamine loss, measured with fluorescent spectroscopy, and dividing this by the initial added concentration (10 mM). The entrapment efficiency of rhodamine B in liposomes were found to be between 4.91 % and 51.54 % based on the number of passes on a microfluidizer. The fifth pass shows a notable lower percent entrapment than the ones passed 1-4 times, with an entrapment efficiency of 4.91 % and 13.70 % (Figure 16). The lower percentage of rhodamine means that some of it was lost during the processing with a microfluidizer.

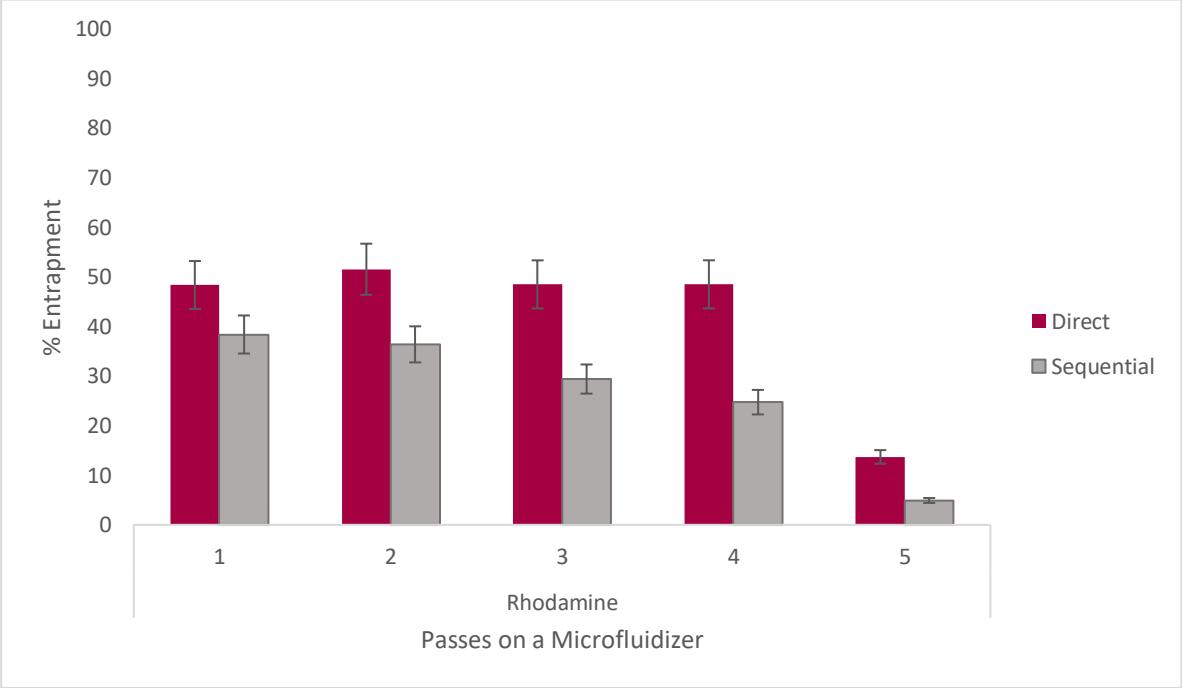


***Figure 16:*** *Entrapment efficiency of rhodamine B in liposomes after 1-5 passes on a microfluidizer. Direct = 1-5 direct passes, Sequential = One pass at a time with 24 hour separation.*

The lower entrapment efficiency of the liposomal dispersion that was passed one at a time, showed a lower entrapment efficiency. This could be explained by the fact that when we are reprocessing we are every time introducing an extra dilution of at minimum 2 mL, coupled with the extra loss of rhodamine every process due to rhodamine adhering to the inlet and the insides of the machine (Figure 17, p. 40). Even with this however, there is a larger drop in the entrapment efficiency at the fifth pass just as with the dispersions that were passed directly.

Since the entrapment values are comparable during the first four passes, it supports the idea that the first pass is responsible for the initial loss of rhodamine, and that further loss is caused by the second lamellarity change that only happened at the fifth pass.

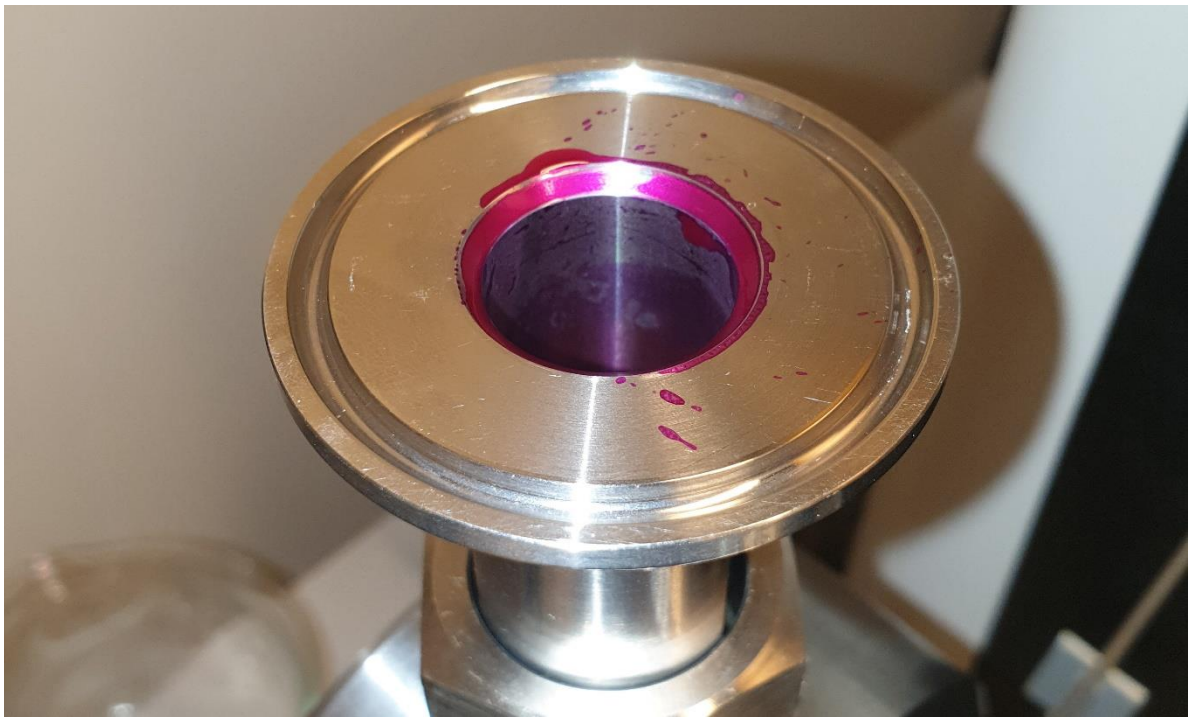

***Figure 17:*** *Inlet of the microfluidizer after processing the rhodamine liposomes. The rhodamine seems to be adhering well to the metal. This is after the sixth cycle, so all the sample had been passed. This shows some loss of material with this processing.*

### 4.1.4 Stability

The stability of a formulation is heavily reliant on their size and surface potential (Hupfeld et al., 2006; Smith et al., 2017). If there are changes to these over time, it can as such be concluded that they are not stable. Due to this, the stability of the rhodamine labeled liposome dispersions were measured based on their size and zeta-potential over the course of 60 days. However already at day 15, the second measurement, the liposomes showed their instability with their deviating zeta potential (Figure 18, p.41). After 45 days, the size also increases past 300 nm, a size not desirable for intravenous drug delivery (Sercombe et al., 2015). The size of all the rhodamine liposomes had increased from approximately 150 nm up to 350 nm from day 0 to day 60 (Figure 19, p. 41), a doubling in size. The zeta-potential showed great variance over time corroborating the formulation instability (Figure 18 & 19, p. 41).

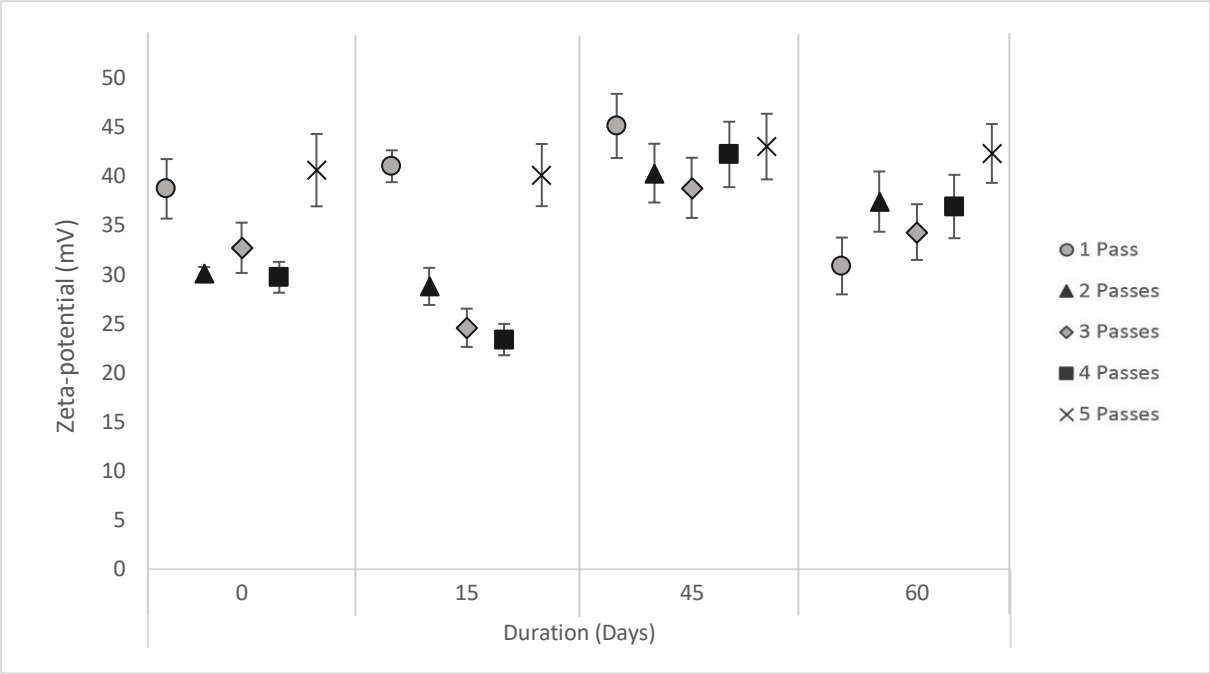


***Figure 18:*** *Development of zeta-potential over the course of 60 days and 4 measurements of rhodamine B liposomes passed 1-5 times on a microfluidizer.*

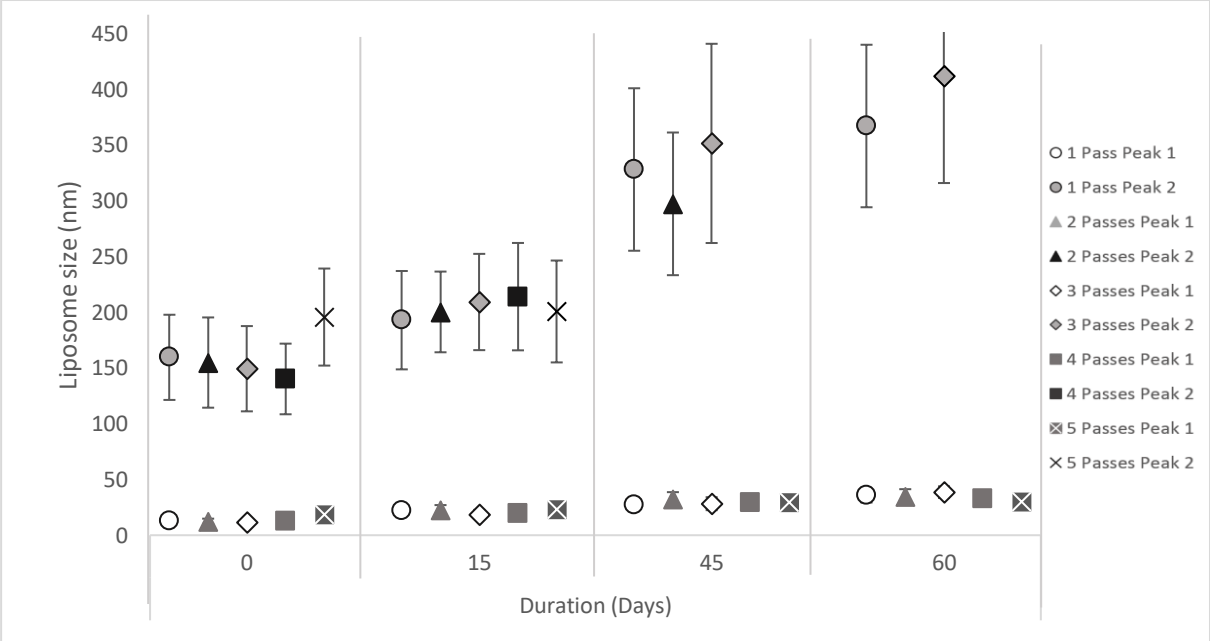


***Figure 19:*** *Development of liposomal size over the course of 60 days and 4 measurements of rhodamine B liposomes passed 1-5 times on a microfluidizer. Some passes (2, 4 and 5) had values above 1000 nm after 45 and/or 60 days. These are not included due to being outside the sensitivity range of the DLS reading.*

The instability of the size can be due to the high polydispersity of these liposomes (Danaei et al., 2018). This polydispersity can lead to agglomeration which the DLS system then sees as one unit (Hupfeld et al., 2006). This agglomeration may happen in unstable dispersions, and

can be due to the fluctuating zeta-potential. This zeta instability might have happened because of changes in pH or to the surface as more rhodamine leaked out of the bilayer and into the aqueous environment.

Because of this instability likely being due to the rhodamine B, it was decided to change the fluorescent compound in the formulation. A compound that was both fluorescent and a pharmacological active ingredient was therefore chosen for the final optimization of a formulation.

## 4.2 Curcumin formulation

For further optimization of the liposomes for imaging purposes, a formulation using a fluorescent compound that was also a pharmacological active substance was considered ideal. This was due to one of the problems concerning imaging using fluorescence, where it is the fluorescent compound that is being traced, and not necessarily the carrier or drug. This due to liposomes leaking their content, like e.g. the fluorophore (Snipstad et al., 2017; Münter et al., 2018). Having our active ingredient be the fluorophore helps overcome this potential limitation. Curcumin is such a molecule (Mahmud et al., 2016) and was for this reason chosen to optimize the liposomal formulation for imaging. This formulation was then furthered by the addition of PEG to develop sterically stabilized liposomes for the improvement of potential circulation time (Monteiro et al., 2014).

### 4.2.1 Size

When passed directly on a microfluidizer for one pass, two dispersions of empty PEGylated liposomes were homogeneous with an average size of 173.7 nm (SD: 44.2 nm) and a PDI of 0.3 (Figure 20, p. 43). This was unexpected due to the non-PEGylated control being highly polydisperse with two size peaks, and there being no membrane modifications other than the introduction of a new type of lipid. When newly prepared these liposomes were very viscus and had a gel-like consistency, after processing they had lost their viscosity. To verify the effect of the initial viscosity on the size distribution, one of these batches was then reprocessed at 15 000 PSI. This reprocessed dispersion was polydisperse with similar size to the non-PEGylated controls. The size of the first peak being 28.92 nm (SD: 5.39 nm) and the second peak 168.7 nm (SD: 31.44). These yielded a higher PDI as well at 0.50 (Figure 20; Table A12 – Appendix).

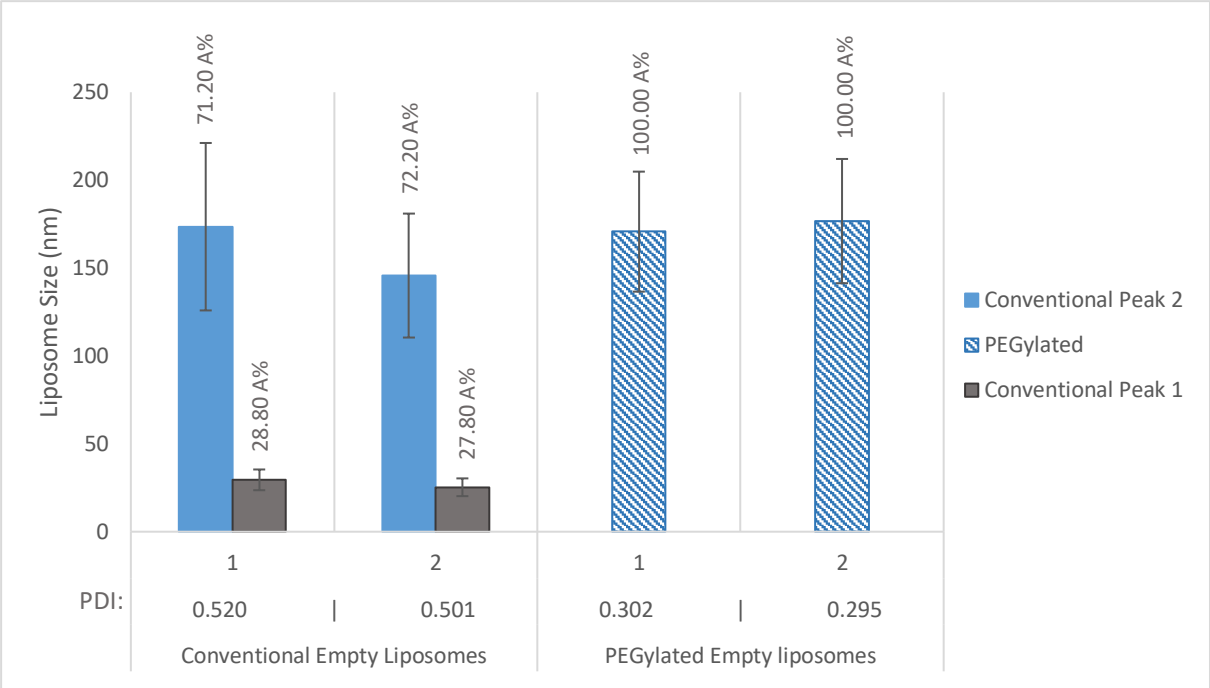


***Figure 20:*** *Size of conventional and PEGylated liposomes after 1 pass on a microfluidizer. The viscous PEGylated liposomes were homogeneous.*

One of the differences between the first and second pass was the viscosity of the initial non processed liposomes. The size and homogeneous liposomes of the first pass was therefore theorized to be at least partially caused by the viscosity of the non-processed PEGylated liposomes.

The size of the curcumin liposomes seemed to have more than one peak during the first readings, with the second and largest peak being around 1-4 µm (Figure 21).

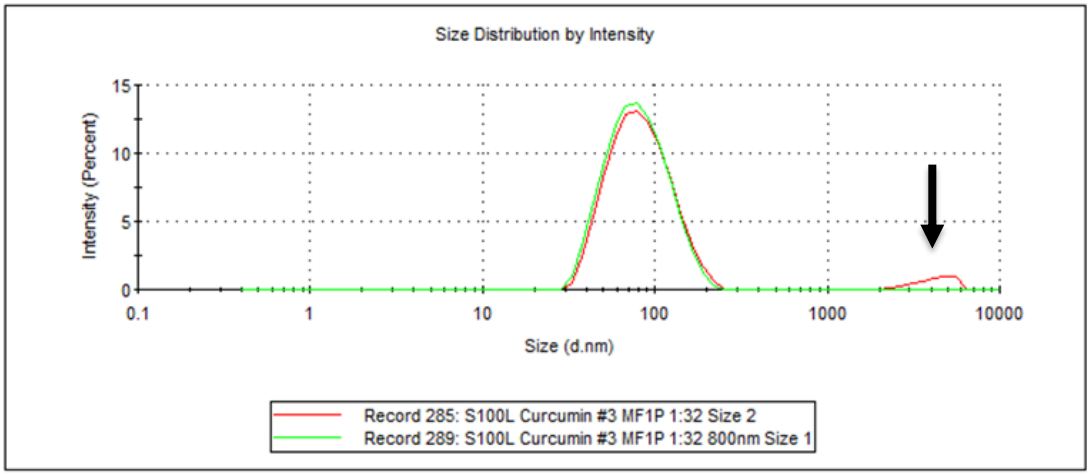


***Figure 21:*** *Size distribution of curcumin liposomes (80.15 nm) after processing with a microfluidizer and after centrifugation and extrusion at 800 nm. Image acquired with Zetasizer nano series SZ.*

However after the removal of free unentrapped curcumin via both centrifugation and membrane filtering, this peak was removed. This meant that this size peak was likely free curcumin, and not liposomes, otherwise the filtration would have had an extrusion effect that would have been measured as a shift in the small peak towards smaller dimensions.

The three curcumin dispersions after processing gave an average size of approximately 75 nm. This system was homogeneous with one size peak and a PDI of approximately 0.25 (Figure 22; Table A10 – Appendix).

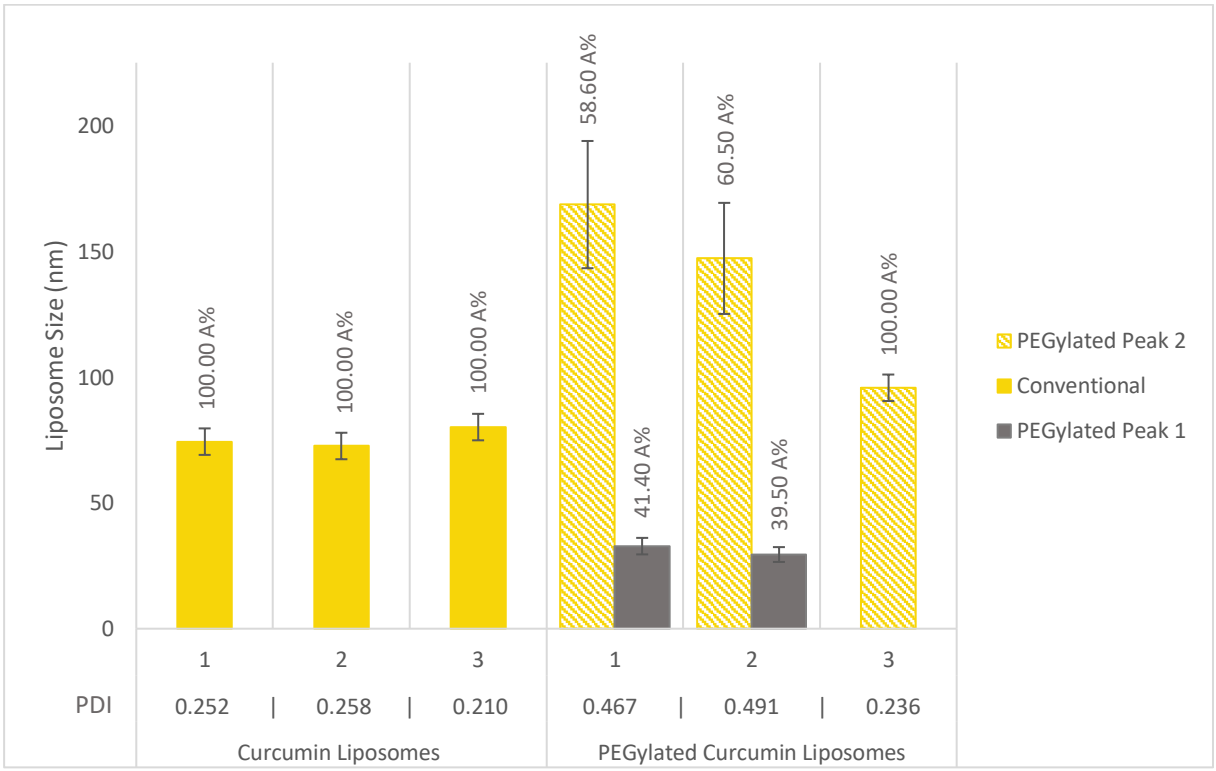


***Figure 22:*** *Size of all three conventional and PEGylated curcumin liposomes after 1 pass on a microfluidizer. A% = Intensity of the size measurement.*

The size of the curcumin liposomes after one pass on the microfluidizer was unexpected as they were smaller than initially predicted. The expectation of a bigger size was largely due to the incorporation of curcumin. Curcumin has been linked to similar effects on the bilayer as cholesterol, due to them having similar membrane interactions (Barry et al., 2008). Since the addition of cholesterol significantly affects the membrane rigidity (Wu et al., 2019), it was suggested that curcumin had some ability to make the liposome bilayer more rigid. The more rigid the bilayer is, the more resistant it is at size reduction (Wu et al., 2019). One pass on the microfluidizer however seems to have given homogeneous SUVs even with the incorporation

of curcumin. This shows that this processing can prepare homogeneous SUVs, very quickly and efficiently and can possibly be done on an industrial level.

The size of the PEGylated curcumin liposomes were after one pass polydisperse with two size peaks, with the first being at 27.84 nm and 31.49 nm (SD: 4.48-6.28 nm) and the second at 147.2 nm and 168.6 nm (SD: 67.84-92.11 nm) (Figure 22, p. 44; Table A14 – Appendix). The PDI was also relatively high at 0.48. This size was also unexpected due to the non-PEGylated curcumin liposomes being homogeneous. These liposomes were then processed again, these passes yielded similar results.

This resulting polydispersity was speculated to be caused by free curcumin interacting with the vesicles during the high sheer in the interaction chamber of the microfluidizer. This was due to there being observed free curcumin in this dispersion before processing, as seen by the orange color appearing after approximately an hour after rehydration of the lipid film (Figure 23). To test this, a third dispersion was made with the same parameters. This was then first sonicated to make the dispersion less viscous, and then centrifuged to get rid of any unentrapped curcumin. The dispersion was after this processed on the microfluidizer once. The resulting system was homogeneous with relatively comparable size to the conventional curcumin liposomes. The size measured was 95.77 nm (SD: 24.00 nm) with a PDI of 0.24 (Figure 22, p. 44; Table A14 – Appendix).

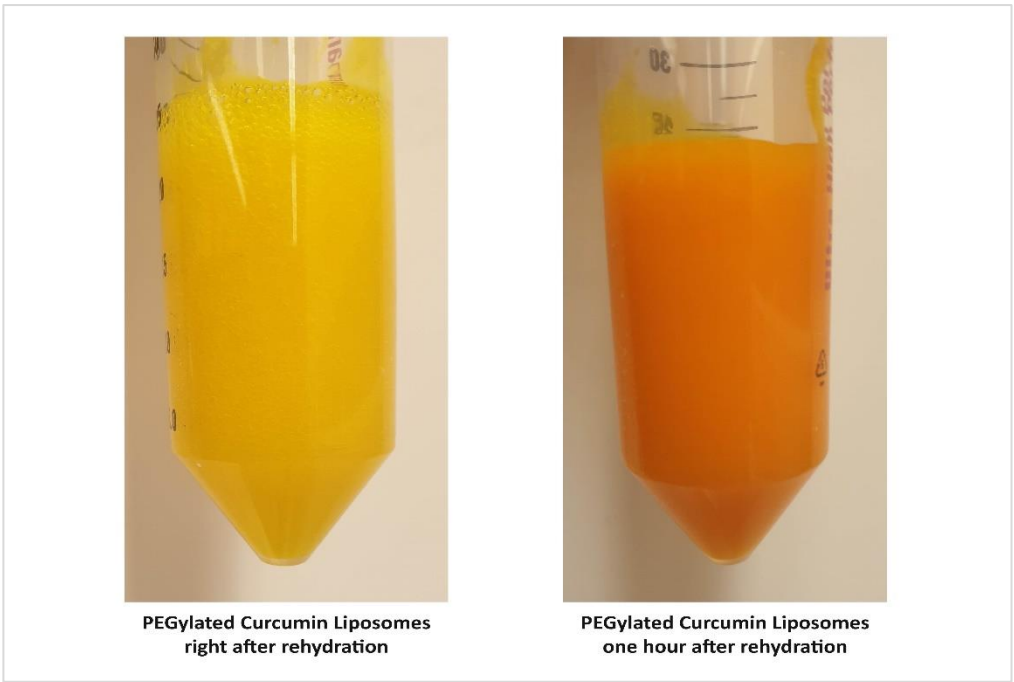


***Figure 23:*** *PEGylated non-processed curcumin liposomes right after preparation (Left) and one hour later (Right).*

The rigidity of the membrane caused by the curcumin might explain why these systems were homogeneous with a low PDI, which were neither achieved with the empty controls nor the rhodamine labeled liposomes. Rigidity seems to resist size reduction down to 20 nm like seen with the other dispersions.

The resulting low polydispersity could be a good predictor of a good stability of these liposomes. Another advantage of rigid or ordered lipid bilayers, is that they have shown to leak less of their content (Wu et al., 2019), which might give a better specificity with fluorescent imaging. This would be due to the higher assurance of curcumin being located in the bilayer, enabling the tracking of the liposomes and not free unentrapped fluorophore.

### 4.2.2 Zeta-potential

Since both curcumin and phospholipids are neutral molecules, a neutral zeta-potential for the curcumin liposomes (± 10 mV) were measured, as expected (Figure 24; Table A11 – Appendix). The small fluctuation in zeta-potential for these neutral liposomes are probably due to possible rearrangement of the lipids (Makino et al., 1991). The incorporation of curcumin in the bilayer does not seem to affect the surface charge when compared to the empty controls. This suggests that curcumin has favorable interactions with the lipids, from within the bilayer itself rather than with its surface.

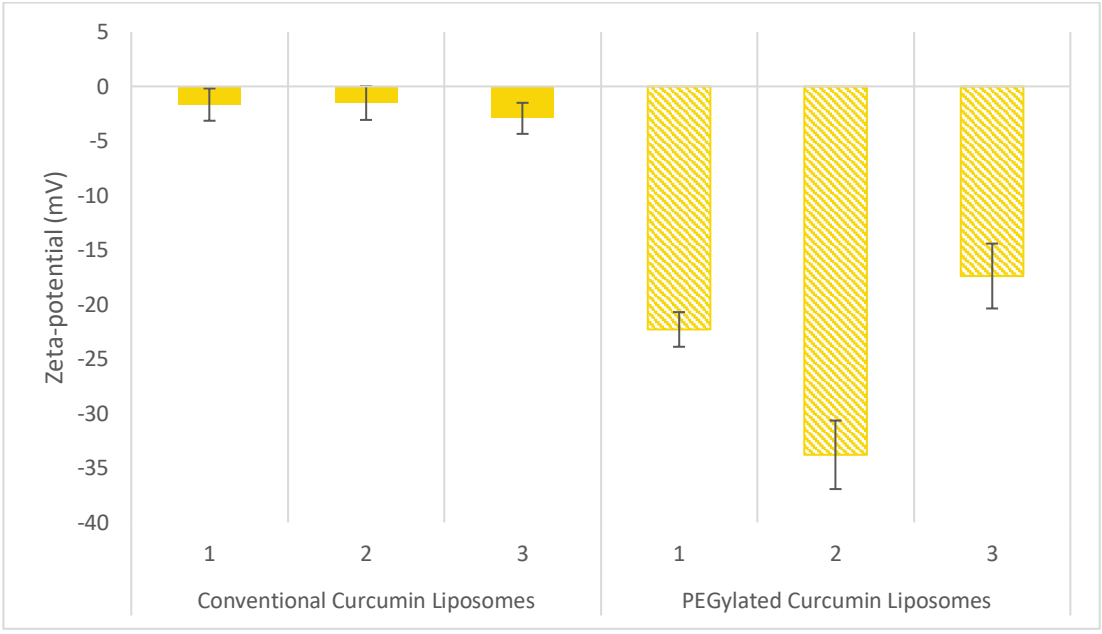


***Figure 24:*** *Measured zeta-potential of all three conventional and PEGylated curcumin liposome dispersions after 1 pass on a microfluidizer.*

The zeta-potential of all the PEGylated liposomes, however, were anionic with values outside of the neutral area (± 10 mV). The zeta-potential measured of the empty liposomes were on average –39.4 mV (SD: 2.66 mV) (Figure 25; Table A13 – Appendix). The zeta-potential of the curcumin ones were similar, but slightly lower at between –17.4 mV and –33.8 mV (Figure 24, p. 46; Table A15 – Appendix).

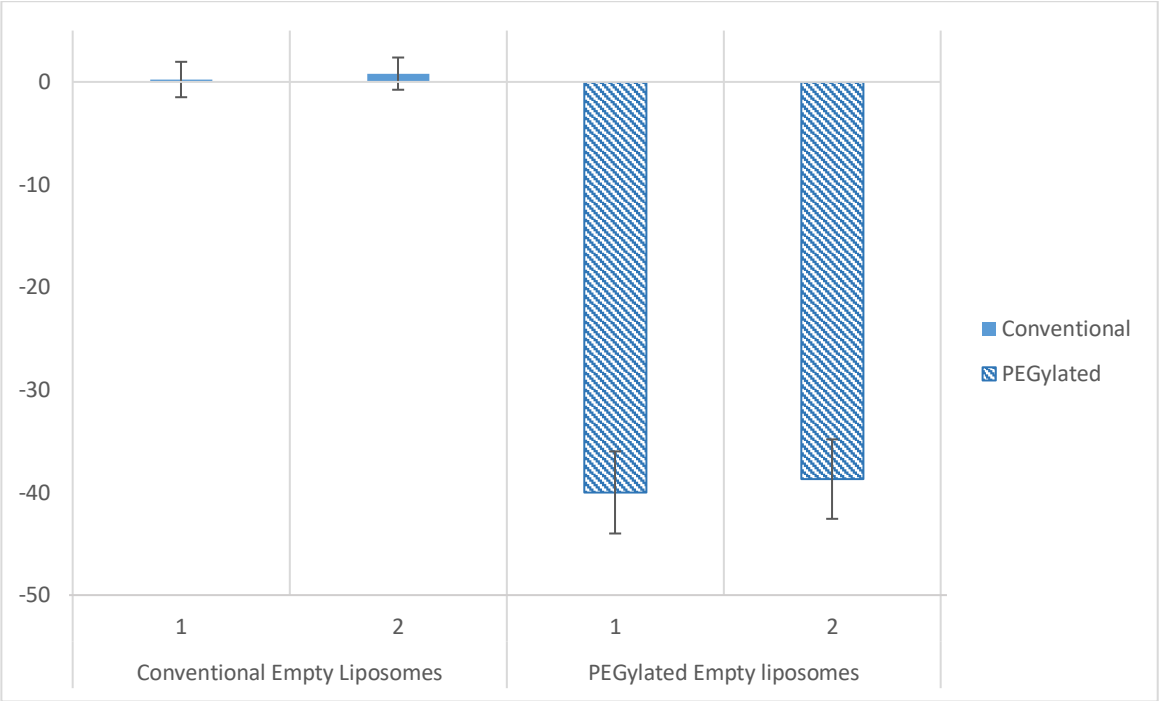


***Figure 25:*** *Measured zeta-potential of conventional and PEGylated liposome dispersions after 1 pass on a microfluidizer.*

Since the zeta-potential indirectly reflects the net charge of the liposome surface, the type of lipids used could potentially have influenced the charge of these liposomal formulations (Tsermentseli et al., 2018). In this case, there seemed to be some surface interactions between the two different lipids (DSPE-PEG and Lipoid S100) that led to a more anionic charge (Figure 24 & 25). These interactions could be due to the high sheer interaction forces from the microfluidizer (Talsma et al., 1994). PEGylated liposomes have been shown to have more anionic zeta-potentials than conventional liposomes (Wolfram et al., 2013), so there might be some interactions between the PEG and the lipids as well that caused this surface charge.

The slightly lower charge of the PEGylated liposomes with curcumin might be due to the stabilizing effect the curcumin has on the lipids (Barry et al., 2008). Because of these favorable interactions and curcumin not being soluble in dH2O, it gives this fluorophore good stability in

the bilayer, which is excellent for the accuracy of fluorescent imaging. Since curcumin is also the drug, imaging these liposomes through fluorescence also increases the specificity, as where the fluorescence is, the drug is as well.

### 4.2.3 Entrapment efficiency curcumin

The entrapment efficiency of curcumin in liposomes was measured to be on average 30.42 % (SD: 3.10 %) (Figure 26).

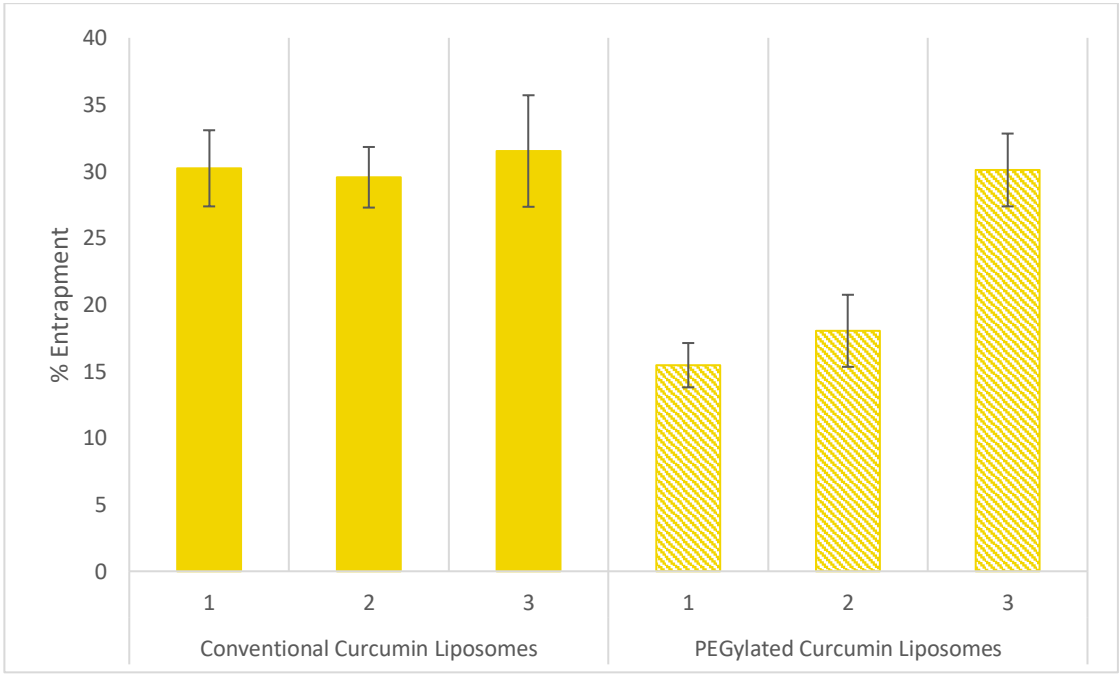


***Figure 26:*** *Entrapment efficiency of curcumin in both conventional and PEGylated liposomes after 1 pass on a microfluidizer.*

The conventional curcumin liposomes were not reprocessed and did not seem to adhere much to the inlet of the microfluidizer. That there was a loss of curcumin however became clear after only a few minutes after processing (Figure 27, p. 49). A gradual sedimentation of the unentrapped curcumin was indeed observed. The previously yellow dispersion became more orange, this color change continued over the course of the next hour until the orange began to separate and sediment and a yellow color became visible once again.

The entrapment efficiency of the third homogeneous PEGylated dispersion was comparable to the curcumin entrapped in the conventional liposomes. The entrapment was measured at 30.10 % (SD: 2.73 %). The other two polydisperse systems had a much lower entrapment efficiency,

at 15.38 % and 17.83 % (SD: 1.66-2.70 %). The third PEGylated and all three of the conventional curcumin dispersions show a comparable amount of encapsulated curcumin (Figure 26, p. 48), which indicates that this value might be dependent on the lipid concentration and liposome size.

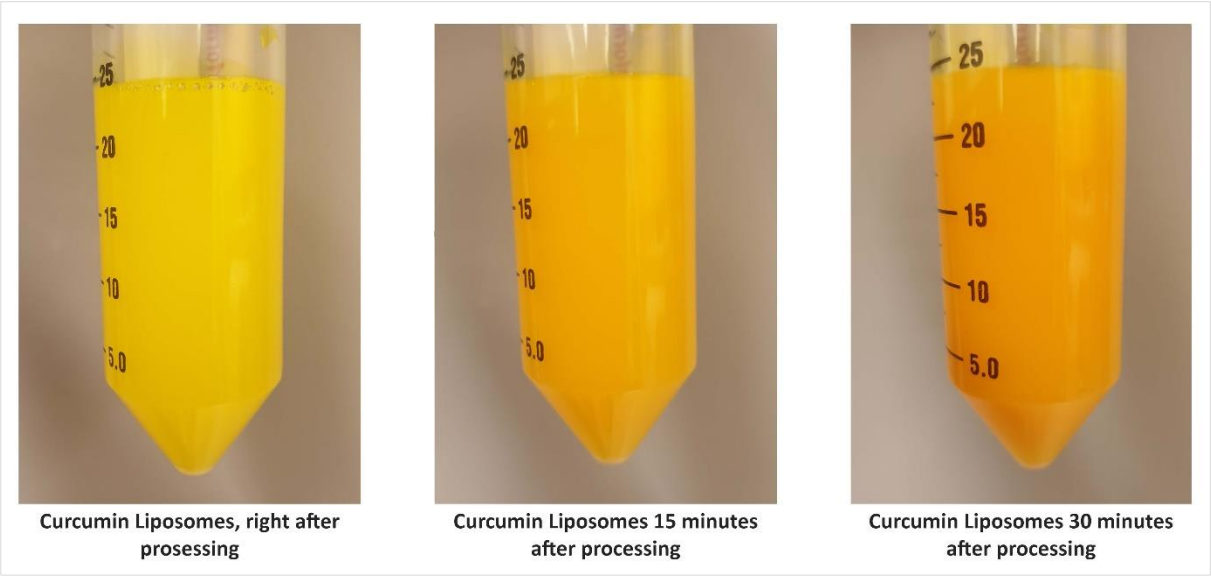


***Figure 27:*** *Conventional curcumin liposomes 0, 15 and 30 minutes after one pass with a microfluidizer*

### 4.2.4 Stability

The stability of the curcumin liposomes were measured based on their size and zeta-potential over the course of 90 days (Hupfeld et al., 2006; Smith et al., 2017). The zeta potential appears stable the first 30 days, however on day 60 there was an increase in zeta-potential to -6.42 mV (Figure 28, p. 50). The surface charge at day 60 is still within the neutral area (± 10 mV), the slightly more negative values can be due to lipid stability and arrangement (Makino et al., 1991) that can change over time because of lipid oxidation (Mosca et al., 2011; Guldiken et al., 2018). The size of these liposomes appear very stable over 90 days (Figure 29, p. 50), due to exhibiting a less than 10 nm increase. In total there is little change in both the zeta-potential and size during 90 days. This indicates a stable dispersion.

The good stability can partially be due to the low polydispersity of the formulation (Danaei et al., 2018), but also the integrity of the lipid membrane due to the increased rigidity. This is because increased rigidity have shown correlation with increased stability (Qi et al., 1996).

Seemingly, PEGylated liposomes showed great initial stability (15 days) which will be followed in the next stages of this project (Figure A1 – Appendix).

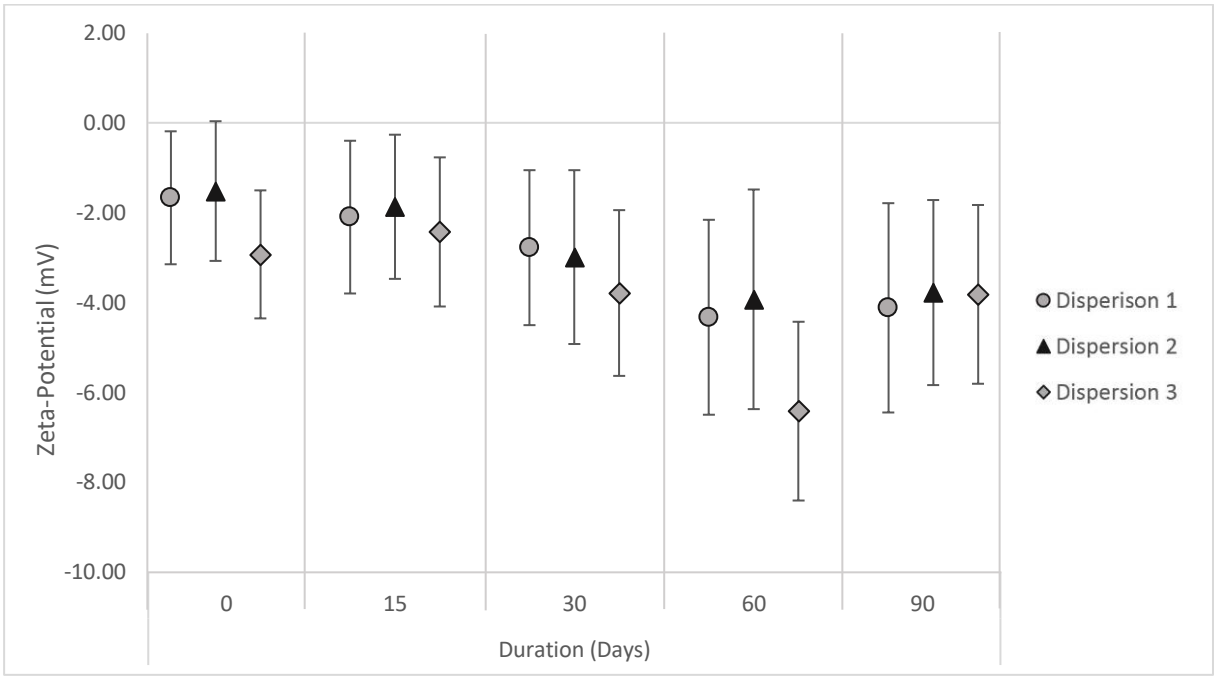


***Figure 28:*** *Development of zeta-potential over the course of 90 days and 5 measurements of conventional curcumin liposomes passed once on a microfluidizer.*

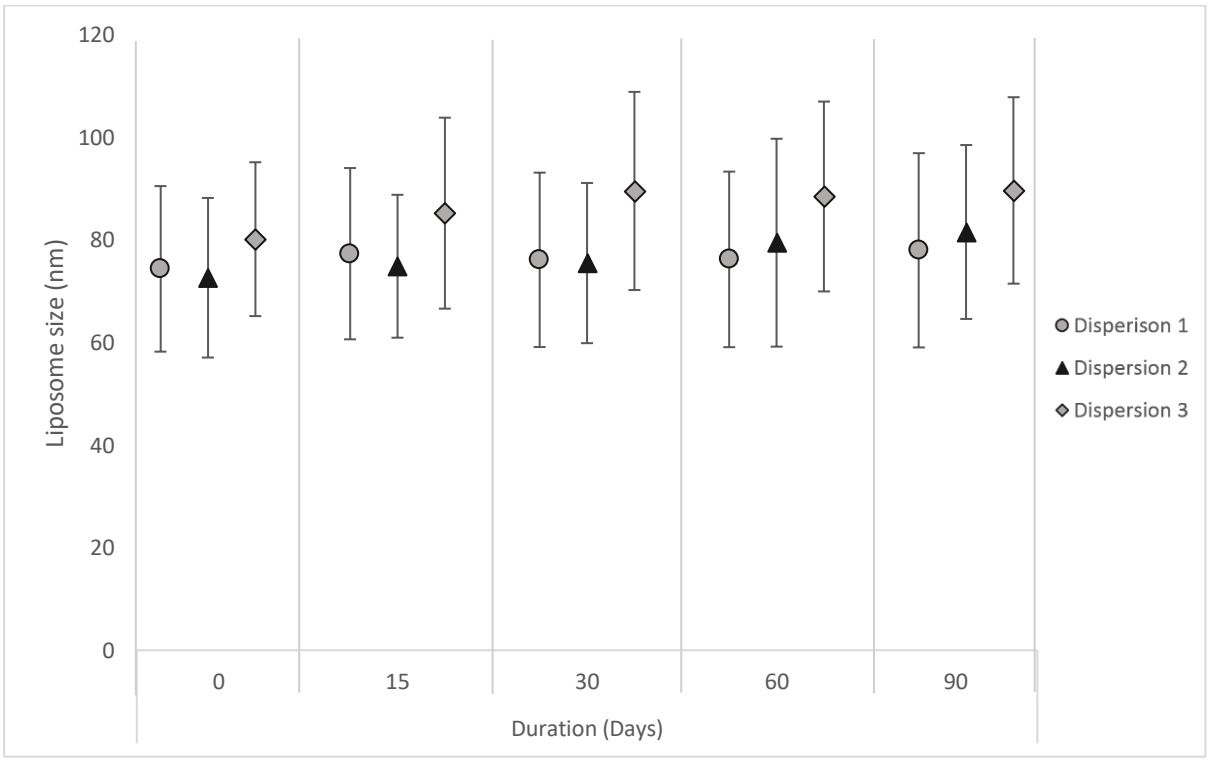


***Figure 29:*** *Development of liposomal size over the course of 90 days and 5 measurements of conventional curcumin liposomes passed once on a microfluidizer.*

## 4.3 Anti-inflammatory activity and cell imaging

Curcumin was chosen for the formulation due to being a pharmacologically active substance in addition to being fluorescent. One of the activities of curcumin is anti-inflammatory activity. Due to the formulation both with and without PEG having nice characteristics, it was decided to test their anti-inflammatory activity in a pilot test.

Some cells that are involved in inflammation, like neutrophils and macrophages release nitric oxide (NO) in high concentrations when inflamed. When produced, NO acts as an inflammatory mediator. Potential changes in NO production from these cells can therefore be used to determine a compounds anti-inflammatory activity. Cells were therefore inflamed to analyze their behavior when treated with curcumin and its formulations. The inflammation was done with LPS, which instigates the production of inducible nitric oxide synthase (iNOS) that converts L-arginine to L-citrulline which produces NO (Sharma et al., 2007; Sadek et al., 2017).

It is not the NO concentration directly that is measured in this step, but rather a complex made with NO which can be used instead. Griess reagent reacts with any NO in the supernatant and generates a pink colored complex measurable with fluorescent spectroscopy. The pinker, the more NO there was prior the addition of the reagent (Tsikas, 2007). Here the NO production of macrophages (RAW 264.7) are measured after inflammation and treatment with curcumin. These cells were also analyzed with flow cytometry and flow-imaged via fluorescence for curcumin uptake.

### 4.3.1 NO production

The NO % was measured with fluorescent spectroscopy. The NO production in the RAW 264.7 macrophages varied between the different treatments (Figure 30, p. 52). The cells treated with water and lower concentrations of DMSO, did not appear to reduce NO production, therefore maintaining their inflammatory status. On the other hand, all the different treatments with curcumin seemed to reduce the NO production, rising with the concentrations added. However so did some of the treatments without curcumin, most notably empty PEGylated liposomes, which reduced the inflammation to the same or higher degree than the liposomes with curcumin (Figure 30, p. 52).

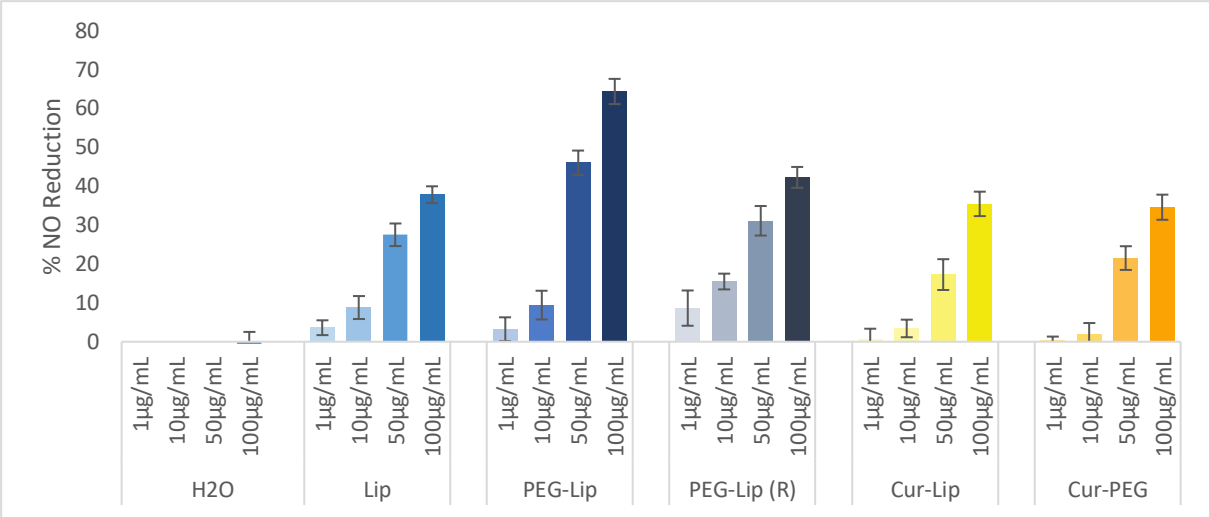


***Figure 30:*** *The NO % reduction of the different liposome formulations with dH2O as control. Lip = liposome, PEG = PEGylated, Cur = curcumin.*

The empty control liposomes reduced the NO production by at most 37.80 % (SD: 2.15 %), the PEGylated control reduced the NO production by 64.32 % (SD: 3.24 %). This is nearly a doubling of the reduction through the addition of PEG. This value was however, thought to be because of the size of these liposomes (173.7 nm) that was not directly comparable with the polydisperse conventional control (27.38 nm and 159.6 nm). This caused the PEGylated control to be extruded and retested. The new size of 94.6 nm (SD: 21.32 nm) showed an NO reduction of 42.24 %, showing a clear size based effect.

Both curcumin formulations (PEGylated and conventional) showed a similar trend of reduction of the inflammatory activity. The cells treated with curcumin dissolved in 30% DMSO showed that curcumin does have some anti-inflammatory activity, with an NO reduction of up to 29.45 % (SD: 2.08 %). When compared to the DMSO control with a reduction of less than 3 % at the highest concentration added, this gives an idea of the anti-inflammatory activity of curcumin (Figure 31, p. 53).

When comparing the effect of the liposomal control with the free curcumin one, no significant synergy was detected. Liposomes have previously shown their tendency to reduce the NO production on inflamed macrophages (Basnet et al., 2012; Giordani et al., 2020). This effect however being greater than the curcumin liposomes was unexpected, as curcumin is known for anti-inflammatory activity (Mahmud et al., 2016), and their ability to inhibit iNOS to reduce NO production (Moran et al., 2012; Prasad et al., 2014).

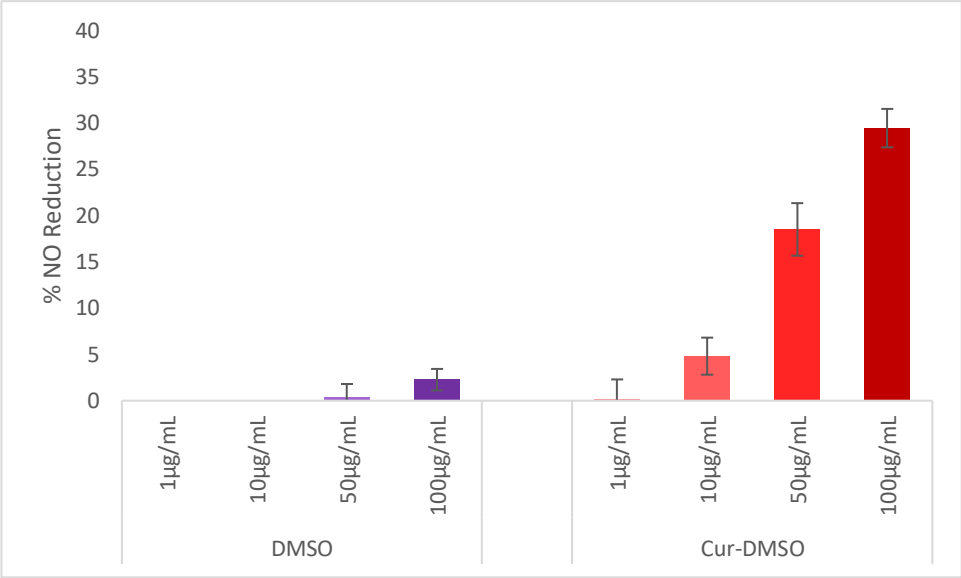


***Figure 31:*** *% NO reduction by curcumin disolved in 30 % DMSO and a corresponding curucmin free DMSO control.*

### 4.3.2 Flow cytometry and cell imaging

Flow cytometry allows for the examination of cell-correlated fluorescence, it was here used to examine if there had been any interaction between curcumin labeled liposomes and macrophages after 24 hours of incubation.

When measuring for the fluorescence in both the FACS and the ISX all the different fluorescence channel were active to tackle the issue of shifting emission that have been reported. In fact, curcumin has a deviating emission spectra based on the medium they are dissolved/dispersed in (Chignell et al., 1994) and its concentrations (Ali et al., 2019). This shifting emission was observed between the 80 % MeOH used for fluorescence detection for the entrapment (542 nm), and just the liposomes without the presence of alcohol (578 nm). The channel V-500 was recognized as most suitable and the internalization results are shown in Figure 32 (p. 54).

The shift of the fluorescence peak after treatment is only minimal. For the empty controls, a fluorescence average of 35 was detected. For the highest concentration of curcumin added (2.0 mg/mL) in the form of conventional liposomes the fluorescence detection was 80.2 (Figure 32A, p.54). For the PEGylated liposomes at the highest concentration, some fluorescence shift was detected, with a value of 122 (Figure 32B). Although looking very carefully a trend in increased fluorescence can be seen (Table 2), the extent of the shift is only in the range of the

so-called unspecific bindings. In fact, any cell culture treated with fluorophores will show a slight shift from its untreated control due to the fluorescent molecules that attach to the cell surface (Bellavancea et al., 2010). As such these results could not be interpreted as definitive proof of internalization.

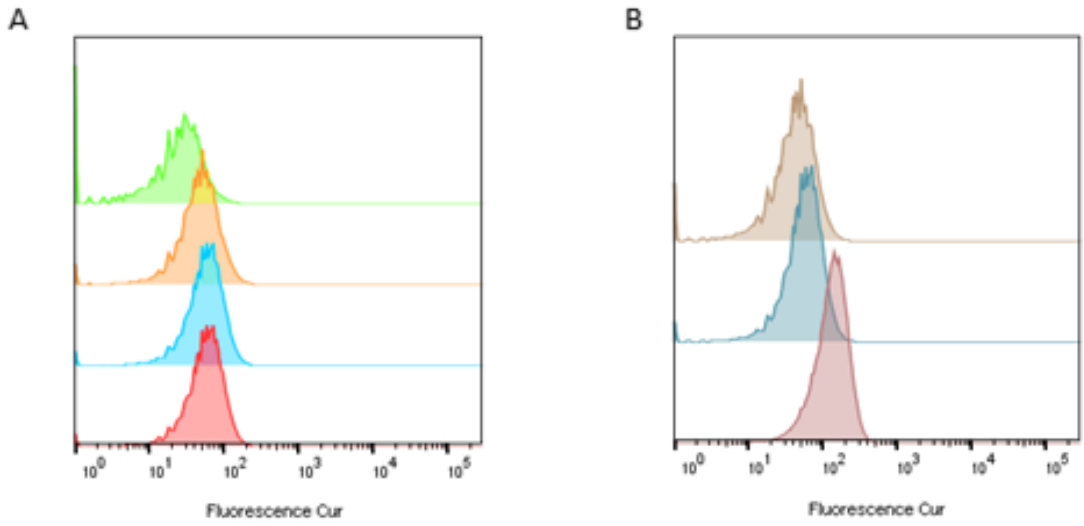


***Figure 32:*** *Fluorescence spectrum in flow cytometry of macrophages after treatment with curcumin and its formulations. Comparison among formulations (A) and concentrations (B). A) Partial overlay of the untreated inflamed cells (bright green), curcumin-loaded liposomes 100 µg/mL of lipids (light blue), PEGylated curcumin-loaded liposomes 100 µg/mL of lipids (bright red) and the correspondent concentration of curcumin in 30% DMSO (bright orange). B) Partial overlay of the untreated inflamed cells (faded brown), PEGylated curcumin-loaded liposomes 100 µg/mL of lipids (faded blue) and PEGylated curcumin-loaded liposomes 1000 µg/mL of lipids (faded red).*

***Table 2:*** **Mean values of fluorescence measured in flow cytometry**

| Formulation | Curcumin concentration | | |
|---|---|---|---|
| | 0 | 0.2 mg/mL | 2 mg/mL |
| Cur-DMSO | - | 24.2 | 32.9 |
| Cur-Lip | 34.9 | 49.9 | 80.2 |
| Cur-PEG | - | 49.5 | 122 |

Note: n=2. Standard deviations are not quantified because the spectra are not symmetric Gaussians. Sample spectra are provided in Figure 32.

To see whether the unspecific binding could be visualized, samples were run in flow imaging. For the curcumin, the fluorescence was expected potentially to be present in several channels. This was channel two (green, 480-560 nm), three (yellow, 560-595 nm) and four (orange, 595-642 nm). All 12 channels were activated to cover the full spectrum, from 435 to 780, but no fluorescence signal could be detected in any (Figure 33, p. 55). Most probably, once

internalized such small liposomes (below the resolution limit), are re-directed inside the cells, in which the overall fluorophore density drastically decreases below the detectable limit. Especially when the dispersion in the medium is combined with a dispatch and elimination (Zhang et al., 2016).

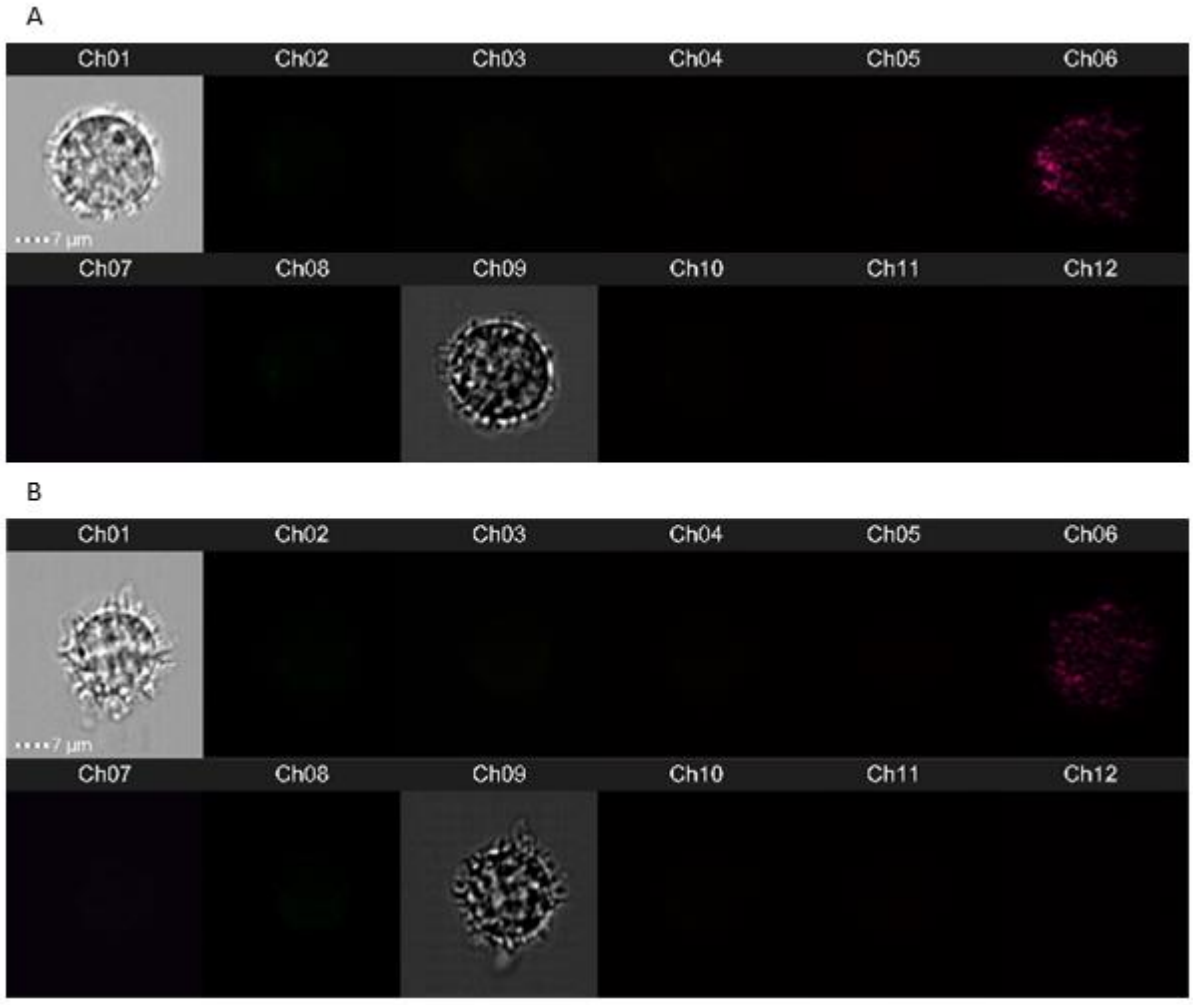


***Figure 33:*** *ISX sample cell imaging. A) Untreated LPS-activated cell. B) Cur-PEG concentration 1000 µg/mL after 24 h incubation. Channels 01 and 09 are bright fields for the synchronization of the two cameras, Channel 06 is a visualization of the side scatter SSC. No brightness adjustments were applied to the images after adjusting the dark background on the auto-fluorescence of the negative control (A).*

From the analysis of the cellular tests, the internalization and the intracellular dispatch of these formulations have yet to be fully understood. Since all the formulation showed an effect on the production of NO in LPS inflamed macrophages, internalization was expected. Because of this, further optimization of imaging could potentially provide some insight on internalization pathways of liposomes for targeting. It could also potentially explain why there is a lack of synergy between the curcumin liposomes and the liposome control.

# 5 Conclusions

We were able to microfluidize liposomes comprised of rather high lipid content and in large volumes. Microfluidized liposomes were smaller in size upon increasing number of passes in microfluidization. However, this kind of processing seems to produce highly variable liposomal dispersions dependent on the composition of the liposomes. Different number of passes affected liposomal characteristics, with lamellar rearrangement not occurring with each pass even though there was an increasing shift towards the smaller liposomes after all passes. The different steps in the processing are therefore important to consider and modify according to the components present in the liposomes. It is as such also important to establish the components that are beneficial or detrimental when choosing the type of processing, such as microfluidization.

After one pass at 10 000 PSI on a microfluidizer, the liposomes were easily reduced in size down to SUVs. These liposomes were either homogeneous or polydisperse systems depending on their composition. The polydisperse systems showed poorer stability as expected, while the homogeneous systems were stable over a long period of time, with higher technological reproducibility.

This liposomal composition determined the liposomal characteristics. The PEGylation made the suspension more viscus, which appeared to improve the performance of the microfluidizer in terms of size and polydispersity. Rhodamine B however had unfavorable effect, exhibiting difficulties in being embedded within the bilayer. Moreover, it could have caused potential toxicity due to the cationic surface charge.

The curcumin on the other hand retained localization in the bilayer, which assures good fluorescence specificity, which can be utilized when examining uptake in cells. The curcumin also contributed to more rigid liposomal membranes, which resulted in more stable homogeneous liposomal dispersions.

This data therefore suggests that for optimizing liposomal processing through a microfluidizer, controlling the viscosity and/or employing a compound that increases rigidity of a liposome membrane is beneficial. If a compound is also fluorescent as well as biologically active such as curcumin, more information on liposomal fate can be gained.

Liposomal curcumin however did not appear to have synergistic effect on NO reduction in LPS-inflamed macrophages, although both carriers and curcumin alone showed the expected anti-inflammatory effect. Flow cytometry and imaging did not provide clear evidences of internalizations and further optimization of the imaging setup is required. Although the results can be seen more as a trend rather than evidence, there is a great potential concerning the curcumin formulations.

# 6 Perspectives

The results of this study show that the components of liposome formulations play a role in the characteristics outcome when processed with a microfluidizer. For the optimization of a microfluidizer, further studies on how the components are beneficial for the microfluidization process might be necessary to replicate outcomes for other future formulations. Curcumin e.g exhibited an increased membrane rigidity in liposomes, another component that does this is cholesterol (Wu et al., 2019). As cholesterol can be added to a variety of formulations, it would as such be interesting to see if the addition of cholesterol gained similar liposomal characteristics to the curcumin liposomes when microfluidized.

There is a great potential in the stable curcumin liposomes, and it could be worth further research. Further imaging optimization would be of interest, e.g. the screening of more incubation endpoints with super-resolution microscopy. This screening might show to be beneficial as this could potentially reveal the mechanisms behind internalization of liposomal curcumin. Curcumin exhibits advantageous biological activities, and knowing their internalization mechanism could make way for better targeted curcumin formulations.

# References


Admin (2014). *Absorption and Fluorescence: Jablonski diagram*. PhotoSynLab (PSL)**:** Jablonski diagram. Retrieved April 20, 2020 from: http://unitedscientists.org/photosynlab/2014/03/08/absorption-and-fluorescence/.

Agarwal, Renu, Igor Iezhitsa, Puneet Agarwal, Nurul Alimah Abdul Nasir, Norhafiza Razali, Renad Alyautdin & Nafeeza Mohd Ismail (2016). *Liposomes in topical ophthalmic drug delivery: an update*. Drug Delivery **23**. DOI: 10.3109/10717544.2014.943336.

Akbarzadeh, Abolfazl, Rogaie Rezaei-Sadabady, Soodabeh Davaran, Sang Woo Joo, Nosratollah Zarghami, Younes Hanifehpour, Mohammad Samiei, Mohammad Kouhi & Kazem Nejati-Koshki (2013). *Liposome: classification, preparation, and applications*. Nanoscale Research Letters **8**. DOI: 10.1186/1556-276X-8-102.

Ali, Zulfiqar, Muhammad Saleem, Babar Manzoor Atta, Sadaf S. Khan & Ghazanfar Hammad (2019). *Determination of curcuminoid content in turmeric using fluorescence spectroscopy*. Spectrochimica Acta Part A: Molecular and Biomolecular Spectroscopy **213**. DOI: 10.1016/j.saa.2019.01.028.

Amreddy, Narsireddy, Anish Babu, Ranganayaki Muralidharan, Janani Panneerselvam, Akhil Srivastava, Rebaz Ahmed, Meghna Mehta, Anupama Munshi & Rajagopal Ramesh (2019). *Recent Advances in Nanoparticle-Based Cancer Drug and Gene Delivery*. Advances in Cancer Research **137**. DOI: 10.1016/bs.acr.2017.11.003.

Bansal, Shyam S., Mehak. Goel, Farrukh Aqil, Manicka V. Vadhanam & Ramesh C. Gupta (2011). *Advanced Drug Delivery Systems of Curcumin for Cancer Chemoprevention*. Cancer Prevention Research **4**. DOI: 10.1158/1940-6207.CAPR-10-0006.

Barry, Jeffrey, Michelle Fritz, Jeffrey R. Brender, Pieter E. S. Smith, Dong-Kuk Lee & Ayyalusamy Ramamoorthy (2008). *Determining the Effects of Lipophilic Drugs on Membrane Structure by Solid-State NMR Spectroscopy: The Case of the Antioxidant Curcumin*. Journal of American Chemical Society **131**. DOI: 10.1021/ja809217u.

Basnet, Purusotam, Haider Hussain, Ingunn Tho & Natasa Skalko-Basnet (2012). *Liposomal Delivery System Enhances Anti-Inflammatory Properties of Curcumin*. Journal Of Pharmaceutical Sciences **101**. DOI: 10.1002/jps.22785.

Bellavancea, Marc-André, Marie-Belle Poirier & David Fortin (2010). *Uptake and intracellular release kinetics of liposome formulations in glioma cells*. International Journal of Pharmaceutics **395**. DOI: 10.1016/j.ijpharm.2010.05.017.

Bian, Xin, Changho Kim & George Em (2016). *111 years of Brownian motion*. Soft Matter **12**. DOI: 10.1039/c6sm01153e.

Boreham, Alexander, Robert Brodwolf, Karolina Walker, Rainer Haag & Ulrike Alexiev (2017). *Time-Resolved Fluorescence Spectroscopy and Fluorescence Lifetime Imaging Microscopy for Characterization of Dendritic Polymer Nanoparticles and Applications in Nanomedicine*. Molecules **22**. DOI: 10.3390/molecules22010017.

Bozzuto, Giuseppina & Agnese Molinari (2015). *Liposomes as nanomedical devices*. International Journal of Nanomedicine **10**. DOI: 10.2147/IJN.S68861.

Brandl, Martin (2007). *Vesicular Phospholipid Gels: A Technology Platform*. Journal of Liposome Research **17**. DOI: 10.1080/08982100601186490.

Chia, Wan Ni, Yan Quan Lee & Kevin Shyong-Wei Tan (2017). *Imaging flow cytometry for the screening of compounds that disrupt the Plasmodium falciparum digestive vacuole*. Methods **112**. DOI: 10.1016/j.ymeth.2016.07.002.

Chignell, C. F., P Bilski, K. J. Reszka, A. G. Motten, R. H. Sik & T. A. Dahl (1994). *Spectral And Photochemical Properties Of Curcumin*. Photochemistry Photobiology **59**. DOI: 10.1111/j.1751-1097.1994.tb05037.x.

Croneya, John C., David M. Jamesona & Robert P. Learmonth (2001). *Fluorescence spectroscopy in biochemistry: teaching basic principles with visual demonstrations* Biochemistry and Molecular Biology Education **29**. DOI: 10.1111/j.1539-3429.2001.tb00071.x.

Danaei, M., M. Dehghankhold, S. Ataei, F. Hasanzadeh Davarani, R. Javanmard, A. Dokhani, Khorasani S. & M. Reza Mozafari (2018). *Impact of Particle Size and Polydispersity Index on the Clinical Applications of Lipidic Nanocarrier Systems*. Pharmaceutics **10**. DOI: 10.3390/pharmaceutics10020057.

Danaei, M., M. Kalantari, M. Raji, H. Samareh Fekri, R. Saber, G. P. Asnani, S. M. Mortazavi, M. R. Mozafari, B. Rasti & A. Taheriazam (2018). *Probing nanoliposomes using single particle analytical techniques: effect of excipients, solvents, phase transition and zeta potential*. Heliyon **4**. DOI: 10.1016/j.heliyon.2018.e01088.

Daraee, Hadis, Ali Etemadi, Mohammad Kouhi, Samira Alimirzalu & Abolfazl Akbarzadeh (2016). *Application of liposomes in medicine and drug delivery*. Artificial Cells, Nanomedicine, and Biotechnology **44**. DOI: 10.3109/21691401.2014.953633.

Dos, Matheus Aparecido, Santos Ramos, Patrícia Bento Da Silva, Larissa Spósito, Luciani Gaspar De Toledo, Bruna Vidal Bonifácio, Camila Fernanda Rodero, Karen Cristina Dos Santos, Marlus Chorilli & Taís Maria Bauab (2018). *Nanotechnology-based drug delivery systems for control of microbial biofilms: a review*. International Journal of Nanomedicine **13**. DOI: 10.2147/IJN.S146195.

Eroğlu, İpek & Mamudu İbrahim (2020). *Liposome–ligand conjugates: a review on the current state of art*. Journal of Drug Targeting **28**. DOI: 10.1080/1061186X.2019.1648479.

Evers, Martijn J. W., Jayesh A. Kulkarni, Roy van der Meel, Pieter R. Cullis, Pieter Vader & Raymond M. Schiffelers (2018). *State-of-the-Art Design and Rapid-Mixing Production Techniques of Lipid Nanoparticles for Nucleic Acid Delivery*. Small **2**: 1700375. DOI: 10.1002/smtd.201700375.

Ganesan, Palanivel, Govindarajan Karthivashan, Shin Young Park, Joonsoo Kim & Dong-Kug Choi (2018). *Microfluidization trends in the development of nanodelivery systems and applications in chronic disease treatments*. International Journal of Nanomedicine **13**. DOI: 10.2147/IJN.S178077.

Gharib, Riham, Hélène Greige-Gerges, Sophie Fourmentin, Catherine Charcosset & Lizette Auezova (2015). *Liposomes incorporating cyclodextrin–drug inclusion complexes: Current state of knowledge*. Carbohydrate Polymers **129**. DOI: 10.1016/j.carbpol.2015.04.048.

Giordani, Barbara, Purusotam Basnet, Ekaterina Mishchenko, Barbara Luppi & Nataša Škalko-Basnet (2020). *Utilizing Liposomal Quercetin and Gallic Acid in Localized Treatment of Vaginal Candida Infections*. Pharmaceutics **12**. DOI: 10.3390/pharmaceutics12010009.

Gomez, Azucena Gonzalez & Zeinab Hosseinidoust (2020). *Liposomes for Antibiotic Encapsulation and Delivery*. ACS Infectious Diseases **6**. DOI: 10.1021/acsinfecdis.9b00357.

Guldiken, Burcu, Monika Gibis, Dilek Boyacioglu, Esra Capanoglu & Jochen Weiss (2018). *Physical and chemical stability of anthocyanin-rich black carrot extractloaded liposomes during storage*. Food Research International **108**. DOI: 10.1016/j.foodres.2018.03.071.

Guo, Peng, Jing Huang, Yaping Zhao, Charles R. Martin, Richard N. Zare & Marsha A. Moses (2018). *Nanomaterial Preparation by Extrusion through Nanoporous Membranes*. Small **14**. DOI: 10.1002/smll.201703493.

Han, Yuanyuan, Yi Gu, Alex Ce Zhang & Yu-Hwa Lo (2016). *Review: Imaging Technologies for Flow Cytometry*. Royal Society of Chemitsry **16**. DOI: 10.1039/c6lc01063f.

Has, C. & P. Sunthar (2019). *A comprehensive review on recent preparation techniques of liposomes*. Journal Of Liposome Research **1**: 1. DOI: 10.1080/08982104.2019.1668010.

Hea, Haisheng, Yi Lua, Jianping Qia, Quangang Zhub, Zhongjian Chenb & Wei Wu (2019). *Adapting liposomes for oral drug delivery*. Acta Pharmaceutica Sinica B **9**. DOI: 10.1016/j.apsb.2018.06.005.

Hua, Susan & Sherry Y. Wu (2013). *The use of lipid-based nanocarriers for targeted pain therapies*. Frontiers in Pharmacology **4**. DOI: 10.3389/fphar.2013.00143.

Hupfeld, Stefan, Ann Holsæter, Merete Skar, Christer B Frantzen & Martin Brandl (2006). *Liposome Size Analysis by Dynamic/Static Light Scattering upon Size Exclusion-/Field*

*Flow-Fractionation*. Journal of Nanoscience and Nanotechnology **6**. DOI: 10.1166/jnn.2006.454.

Ingebrigtsen, Sveinung G., Nataša Škalko-Basnet, Cristiane de Albuquerque Cavalcanti Jacobsen & Ann Mari Holsæter (2017). *Successful co-encapsulation of benzoyl peroxide and chloramphenicol in liposomes by a novel manufacturing method - dual asymmetric centrifugation*. European Journal of Pharmaceutical Sciences **97**. DOI: 10.1016/j.ejps.2016.11.017.

Jøraholmen, May Wenche, Purusotam Basnet, Ganesh Acharya & Nataša Škalko-Basnet (2017). *PEGylated liposomes for topical vaginal therapy improve delivery of interferon alpha*. Journal of Pharmaceutics and Biopharmaceutics **113**. DOI: 10.1016/j.ejpb.2016.12.029.

Jøraholmen, May Wenche, Purusotam Basnet, Mia Jonine Tostrup, Sabrin Moueffaq & Nataša Škalko-Basnet (2019). *Localized Therapy of Vaginal Infections and Inflammation: Liposomes-In-Hydrogel Delivery System for Polyphenols*. Pharmaceutics **11**. DOI: 10.3390/pharmaceutics11020053.

Kanasova, Maria & Karel Nesmerak (2017). *Systematic review of liposomes' characterization methods*. Monatsh Chem **148**. DOI: 10.1007/s00706-017-1994-9.

Khan, Avik, Khanh Dang Vu, Gregory Chauve, Jean Bouchard, Bernard Riedl & Monique Lacroix (2014). *Optimization of microfluidization for the homogeneous distribution of cellulose nanocrystals (CNCs) in biopolymeric matrix*. Cellulose **21**. DOI: 10.1007/s10570-014-0361-9.

Kunwar, Amit, Atanu Barik, Ruchi Pandey & K. Indira Priyadarsini (2006). *Transport of liposomal and albumin loaded curcumin to living cells: An absorption and fluorescence spectroscopic study*. Biochimica et Biophysica Acta (BBA) **1760**. DOI: 10.1016/j.bbagen.2006.06.012.

Lammers, Twan, Silvio Aime, Wim E. Hennink, Gert Storm & Fabian Kiessling (2011). *Theranostic Nanomedicine*. Accounts Of Chemical Research **44**. DOI: 10.1021/ar200019c.

Lichtman, Jeff W. & José-Angel Conchello (2005). *Fluorescence microscopy*. Nature Methods **2**. DOI: 10.1038/NMETH817.

Lu, Kong-Jun, Wei Wang, Xiao-Ling Xu, Fei-Yang Jin, Jing Qi, Xiao-Juan Wang, Xu-Qi Kang, Meng-Lu Zhu, Qiao-Ling Huang, Chao-Heng Yu, Jian You & Yong-Zhong Du (2019). *A dual deformable liposomal ointment functionalized with retinoic acid and epidermal growth factor for enhanced burn wound healing therapy*. Biomaterials Science **7**. DOI: 10.1039/c8bm01569d.

Mahmud, Mohamed, Adriana Piwoni, Nina Filipczak, Martyna Janicka & Jerzy Gubernator (2016). *Long-Circulating Curcumin-Loaded Liposome Formulations with High*

*Incorporation Efficiency, Stability and Anticancer Activity towards Pancreatic Adenocarcinoma Cell Lines In Vitro*. PLOS One **11**. DOI: 10.1371/journal.pone.0167787.

Makino, Kimiko, Takeshi Yamada, Mariko Kimura, Takashi Oka, Hiroyuki Ohshima & Tamotsu Kondo (1991). *Temperature- and ionic strength-induced conformational changes in the lipid head group region of liposomes as suggested by zeta potential data* Biophysical Chemistry **41**. DOI: 10.1016/0301-4622(91)80017-L.

Martina, Marie-Sophie, Jean-Paul Fortin, Laure Fournier, Christine Me´nager, Florence Gazeau, Olivier Cle´ment & Sylviane Lesieur (2007). *Magnetic Targeting of Rhodamine-Labeled Superparamagnetic Liposomes to Solid Tumors: In Vivo Tracking by Fibered Confocal Fluorescence Microscopy*. Molecular Imaging **6**. DOI: 10.2310/7290.2007.00004.

Matos, Carla, Baltazar de Castro, Paula Gameiro, Jose´ L. F. C. Lima & Salette Reis (2003). *Zeta-Potential Measurements as a Tool To Quantify the Effect of Charged Drugs on the Surface Potential of Egg Phosphatidylcholine Liposomes*. Langmuir **20**. DOI: 10.1021/la034780b.

Monteiro, Nelson, Albino Martins, Rui L. Reis & Nuno M. Neves (2014). *Liposomes in tissue engineering and regenerative medicine*. Journal of the Royal Society Interface **11**. DOI: 10.1098/rsif.2014.0459.

Moran, Jose M., Raul Roncero-Martin, Francisco J. Rodriguez-Velasco, Julian F. Calderon-Garcia, Purificacion Rey-Sanchez, Vicente Vera, Maria L. Canal-Macias & Juan D. Pedrera-Zamorano (2012). *Effects of Curcumin on the Proliferation and Mineralization of Human Osteoblast-Like Cells: Implications of Nitric Oxide*. International Journal of Molecular Sciences **13**. DOI: 10.3390/ijms131216104.

Mosca, Monica, Andrea Ceglie & Luigi Ambrosone (2011). *Effect of membrane composition on lipid oxidation in liposomes*. Chemistry and Physics of Lipids **164**. DOI: 10.1016/j.chemphyslip.2010.12.006.

Mozuraitytea, Revilija, Turid Rustada & Ivar Storrø (2006). *Oxidation of cod phospholipids in liposomes: Effects of salts, pH and zeta potential*. European Journal of Lipid Science and Technology **108**. DOI: DOI 10.1002/ejlt.200600139.

Münter, Rasmus, Kasper Kristensen, Dennis Pedersbæk, Jannik Bruun Larsen, Jens Bæk Simonsen & Thomas Lars Andresen (2018). *Dissociation of fluorescently labeled lipids from liposomes in biological environments challenges the interpretation of uptake studies*. Nanoscale **10**. DOI: 10.1039/C8NR07755J.

Park, Youngjin, Isabel S. Abihssira-García, Sebastian Thalmann, Geert F. Wiegertjes, Daniel R. Barreda, Pål A. Olsvik & Viswanath Kiron (2020). *Imaging Flow Cytometry Protocols for Examining Phagocytosis of Microplastics and Bioparticles by Immune Cells of Aquatic Animals*. Frontiers in Immunology **11**. DOI: 10.3389/fimmu.2020.00203.

Pastorino, Fabio, Chiara Brignole, Daniela Di Paolo, Patrizia Perri, Flavio Curnis, Angelo Corti & Mirco Ponzoni (2019). *Overcoming Biological Barriers in Neuroblastoma Therapy: The Vascular Targeting Approach with Liposomal Drug Nanocarriers*. Small **15**: 1804591. DOI: 10.1002/smll.201804591.

Patil, Yogita P. & Sameer Jadhav (2013). *Novel methods for liposome preparation*. Chemistry and Physics of Lipids **8**. DOI: 10.1016/j.chemphyslip.2013.10.011.

Patra, Jayanta K., Gitishree Das, Leonardo F. Fraceto, Estefania V. R. Campos, Maria del Pilar Rodriguez-Torres, Laura S. Acosta-Torres, Luis A. Diaz-Torres, Renato Grillo, Mallappa K. Swamy, Shivesh Sharma, Solomon Habtemariam & Han-Seung Shin (2018). *Nano based drug delivery systems: recent developments and future prospects*. Journal of Nanobiotechnology **16**. DOI: 10.1186/s12951-018-0392-8.

Pereira, Hugo, Peter S.C. Schulzeb, Lisa Maylin Schüler, Tamára Santos, Luísa Barreira & João Varela (2018). *Fluorescence activated cell-sorting principles and applications in microalgal biotechnology*. Algal Research **30**. DOI: 10.1016/j.algal.2017.12.013.

Prasad, Sahdeo, Amit K. Tyagi & Bharat B. Aggarwal (2014). *Recent Developments in Delivery, Bioavailability, Absorption and Metabolism of Curcumin: the Golden Pigment from Golden Spice*. Cancer Research and Treatment **46**. DOI: 10.4143/crt.2014.46.1.2.

Rodrigues, Letícia, Fabian Schneider, Xiaohan Zhang, Elin Larsson, Lindon W.K. Moodie, Hendrik Dietz, Christine M. Papadakis, Gerhard Winter, Richard Lundmark & Madlen Hubert (2019). *Cellular uptake of self-assembled phytantriol-based hexosomes is independent of major endocytic machineries*. Journal of Colloid and Interface Science **553**. DOI: 10.1016/j.jcis.2019.06.045.

Sadek, Maiada M., Mina Barzegar Amiri Olia, Cameron J. Nowell, Nicholas Barlow, Carl H. Schiesser, Sandra E. Nicholson & Raymond S. Norton (2017). *Characterisation of a novel coumarin-based fluorescent probe for monitoring nitric oxide production in macrophages*. Bioorganic & Medicinal Chemistry **25**. DOI: 10.1016/j.bmc.2017.08.054.

Schuh, Roselena S., Édina Poletto, Flávia N. S. Fachel, Ursula Matte, Guilherme Baldo & Helder F. Teixeira (2018). *Physicochemical properties of cationic nanoemulsions and liposomes obtained by microfluidization complexed with a single plasmid or along with an oligonucleotide: Implications for CRISPR/Cas technology*. Journal of Colloid and Interface Science **530**. DOI: 10.1016/j.jcis.2018.06.058.

Sercombe, Lisa, Tejaswi Veerati, Fatemeh Moheimani, Sherry Y. Wu, Anil K. Sood & Susan Hua (2015). *Advances and Challenges of Liposome Assisted Drug Delivery*. Frontiers in Pharmacology **6**. DOI: 10.3389/fphar.2015.00286.

Sharma, J. N., A. Al-Omran & S. S. Parvathy (2007). *Role of nitric oxide in inflammatory diseases*. Inflammopharmacology **15**. DOI: 10.1007/s10787-007-0013-x.

Sigma-Aldrich. (2019). *Curcumin*. Retrieved Novebmer 7, 2019 from: https://www.sigmaaldrich.com/catalog/product/sial/28260?lang=en&region=NO.

Sigma-Aldrich. (2019). *Rhodamine B, for fluorescence*. Retrieved October 21, 2019 from: https://www.sigmaaldrich.com/catalog/product/sigma/83689?lang=en&region=NO.

Smith, Mackensie C., Rachael M. Crist, Jeffrey D. Clogston & Scott E. McNeil (2017). *Zeta potential: a case study of cationic, anionic, and neutral liposomes*. Analytical and Bioanalytical Chemistry **409**. DOI: 10.1007/s00216-017-0527-z.

Snipstad, Sofie, Sjoerd Hak, Habib Baghirov, Einar Sulheim, Yrr Mørch, Sylvie Lelu, Eva von Haartman, Marcus Bäck, K. Peter R. Nilsson, Andrey S. Klymchenko, Catharina de Lange Davies & Andreas K. O. Åslund (2017). *Labeling Nanoparticles: Dye Leakage and Altered Cellular Uptake*. International Society for Advancement of Cytometry **91**. DOI: 10.1002/cyto.a.22853.

Sriwongsitanont, Supaporn & Masaharu Ueno (2004). *Effect of a PEG lipid (DSPE-PEG2000) and freeze-thawing process on phospholipid vesicle size and lamellarity*. Colloid and Polymer Science **282**. DOI: 10.1007/s00396-003-1015-x.

Taciak, Bartłomiej, Maciej Białasek, Agata Braniewska, Zuzanna Sas, Paulina Sawicka, Łukasz Kiraga, Tomasz Rygiel & Magdalena Kro (2018). *Evaluation of phenotypic and functional stability of RAW 264.7 cell line through serial passages*. PLOS One **13**. DOI: 10.1371/journal.pone.0198943.

Talsma, Herre, Yekta A. Ozer, Louis Van Bloois & Daan Crommelin (1994). *The Size Reduction of Liposomes with a High Pressure Homogenizer (Microfluidizer™). Characterization of Prepared Dispersions and Comparison with Conventional Methods.* Drug Development And Industrial Pharmacy **15**. DOI: 10.3109/03639048909040205.

Ternullo, Selenia, Louis de Weerd, Ann Mari Holsæter, Gøril Eide Flaten & Nataša Škalko-Basnet (2017). *Going skin deep: A direct comparison of penetration potential of lipid-based nanovesicles on the isolated perfused human skin flap model*. European Journal of Pharmaceutics and Biopharmaceutics **121**. DOI: 10.1016/j.ejpb.2017.09.006.

Ternullo, Selenia, Laura Victoria Schulte Werning, Ann Mari Holsæter & Nataša Škalko-Basnet (2019). *Curcumin-In-Deformable Liposomes-In-ChitosanHydrogel as a Novel Wound Dressing*. Pharmaceutics **12**. DOI: 10.3390/pharmaceutics12010008.

Tsermentseli, Stella K., Konstantinos N. Kontogiannopoulos, Vassilios P. Papageorgiou & Andreana N. Assimopoulou (2018). *Comparative Study of PEGylated and Conventional Liposomes as Carriers for Shikonin.* Fluids **3**. DOI: 10.3390/fluids3020036.

Wagner, Andreas & Karola Vorauer Uhl (2010). *Liposome Technology for Industrial Purposes*. Journal of Drug Delivery **2011**. DOI: 10.1155/2011/591325.

Wayne, Elizabeth C., Christian Long, Matthew J. Haney, Elena V. Batrakova, Tina M. Leisner, Leslie V. Parise & Alexander V. Kabanov (2019). *Targeted Delivery of siRNA Lipoplexes to Cancer Cells Using Macrophage Transient Horizontal Gene Transfer*. Advanced Science **6**. DOI: 10.1002/advs.201900582.

Wilczewska, Agnieszka Z., Katarzyna Niemirowicz, Karolina H. Markiewicz & Halina Car (2012). *Nanoparticles as drug delivery systems*. Nanoparticles and drugs **64**. DOI: 10.1016/s1734-1140(12)70901-5.

Wolfram, Joy, Krishna Suri, Yong Yang, Jianliang Shen, Christian Celia, Massimo Fresta, Yuliang Zhao, Haifa Shen & Mauro Ferrari (2013). *Shrinkage of pegylated and non-pegylated liposomes in serum*. Colloids and Surfaces B: Biointerfaces **114**. DOI: 10.1016/j.colsurfb.2013.10.009.

Wu, Hangyi, Miaorong Yu, Yunqiu Miao, Shufang He, Zhuo Dai, Wenyi Song, Yuan Liu, Sha Song, Ejaj Ahmad, Dongkai Wang & Yong Gan (2019). *Cholesterol-tuned liposomal membrane rigidity directs tumor penetration and anti-tumor effect*. Acta Pharmaceutica Sinica B **9**. DOI: 10.1016/j.apsb.2019.02.010.

Zahednezhada, Fahimeh, Maryam Saadata, Hadi Valizadehb, Parvin Zakeri-Milanic & Behzad Baradaran (2019). *Liposome and immune system interplay: Challenges and potentials*. Journal of Controlled Release **305**: 194. DOI: 10.1016/j.jconrel.2019.05.030.

Zhang, Haisong, Meng Yu, Hailei Zhang, Libin Bai, Yonggang Wu, Sujuan Wang & Xinwu Ba (2016). *Synthesis, characterization and fluorescent properties of water-soluble glycopolymer bearing curcumin pendant residues*. Bioscience, Biotechnology, and Biochemistry **80**. DOI: 10.1080/09168451.2016.1171696.

# Appendix

## Preparation of liposomes

***Table A 1:*** **Composition and processing of empty liposomes**

| Batch | Processing | Volume | SPC | Concentration |
|---|---|---|---|---|
| | | [mL] | [mg] | [mg/mL] |
| **1** | 1 Pass | 22 | 600 | 27.3 |
| **2** | 1 Pass | 22 | 600 | 27.3 |

***Table A 2:*** **Composition and processing of empty PEGylated liposomes**

| Batch | Processing | Volume | S-100 | | PEG-DSPE | | SPC | |
|---|---|---|---|---|---|---|---|---|
| | | [mL] | [mg] | [mg/mL] | [mg] | [mg/mL] | [mg] | [mg/mL] |
| **1** | 1-2 Passes | 22 | 570 | 25.90 | 111.1 | 5.05 | 681 | 31.00 |
| **2** | 1 Pass | 22 | 570 | 25.90 | 111.2 | 5.06 | 681 | 31.00 |

***Table A 3:*** **Composition and processing of rhodamine B liposomes**

| Batch | Processing | | Volume | S-100 | | Rhodamine B | | | Rhodamine B/SPC |
|---|---|---|---|---|---|---|---|---|---|
| | | | [mL] | [mg] | [mg/mL] | [mg] | [mM] | [mg/mL] | - |
| 1 | Sonicated | 2 min | 47.90 | 10.00 | 300.00 | 4.79 | 10.00 | 30.00 | 0.160 |
| 2 | Sonicated | 2 min | 47.90 | 10.00 | 300.00 | 4.79 | 10.00 | 30.00 | 0.2160 |
| 3 | Extruded | 4 x 80nm | 47.90 | 5.00 | 300.00 | 4.79 | 10.00 | 30.00 | 0.160 |
| | Sonicated | 1 min | | 5.00 | | | | | |
| 4 | Microfluidized | 5 Passes | 95.80 | 20.00 | 600.00 | 4.79 | 10.00 | 30.00 | 0.160 |
| 5 | Microfluidized | 1-5 Passes | 95.80 | 20.00 | 600.00 | 4.79 | 10.00 | 30.00 | 0.160 |
| 6 | Microfluidized | 1 Pass | 95.80 | 22.00 | 600.00 | 4.35 | 9.09 | 27.27 | 0.160 |
| 7 | Microfluidized | 2 Passes | 95.80 | 22.00 | 600.00 | 4.35 | 9.09 | 27.27 | 0.160 |
| 8 | Microfluidized | 3 Passes | 95.80 | 22.00 | 600.00 | 4.35 | 9.09 | 27.27 | 0.160 |
| 9 | Microfluidized | 4 Passes | 95.80 | 22.00 | 600.00 | 4.35 | 9.09 | 27.27 | 0.160 |

***Table A 4:*** **Composition and processing of Curcumin liposomes**

| Batch | Processing | | Volume | S-100 | | Curcumin | | Curcumin/SPC |
|---|---|---|---|---|---|---|---|---|
| | | | [mL] | [mg] | [mg/mL] | [mg] | [mg/mL] | [mg/mL] |
| **1** | Microfluidized | 1 Pass | 22 | 600 | 27.27 | 60 | 2.73 | 0.10 |
| **2** | Microfluidized | 1 Pass | 22 | 600 | 27.27 | 60 | 2.73 | 0.10 |
| **3** | Microfluidized | 1 Pass | 22 | 600 | 27.27 | 60 | 2.73 | 0.10 |

***Table A 5:*** **Composition and processing of PEGylated Curcumin liposomes**

| Batch | Processing | Volume | S-100 | | PEG-DSPE | | Curcumin | | SPC | |
|---|---|---|---|---|---|---|---|---|---|---|
| | | [mL] | [mg] | [mg/mL] | [mg] | [mg/mL] | [mg] | [mg/mL] | [mg] | [mg/mL] |
| **1** | 1-2 Passes | 22 | 570 | 25.9 | 111.0 | 5.05 | 60 | 2.73 | 681 | 31.00 |
| **2** | 1 Pass | 22 | 570 | 25.9 | 111.0 | 5.05 | 60 | 2.73 | 681 | 31.00 |

## Characterizations

***Table A 6:*** **Size and size distributions of empty liposomes after one pass on a microfluidizer**

| | | Peak 1 | | | | Peak 2 | | | |
|---|---|---|---|---|---|---|---|---|---|
| Batch | Processing | Size | SD | A | PDI | Size | SD | A | PDI |
| | Microfluidizer | [nm] | [nm] | [%] | - | [nm] | [nm] | [%] | - |
| 1 | 1 Pass | 29.49 | 5.12 | 28.8 | 0.52 | 0.52 | 47.64 | 71.20 | 0.52 |
| 2 | 1 Pass | 25.27 | 3.96 | 27.8 | 0.50 | 0.50 | 35.26 | 72.20 | 0.50 |

***Table A 7:*** **Zeta-potential of empty liposomes after one pass on a microfluidizer**

| | | Zeta-Potential | |
|---|---|---|---|
| Batch | Processing | Mean charge | SD |
| | Microfluidizer | [mV] | [mV] |
| 1 | 1 pass | 0.232 | 1.73 |
| 2 | 1 pass | 0.806 | 1.57 |

***Table A 8:*** **Size and size distributions of rhodamine B liposomes after processing on a microfluidizer for 1 - 5 passes**

| | | Peak 1 | | | | Peak 2 | | | |
|---|---|---|---|---|---|---|---|---|---|
| Batch | Processing | Size | SD | A | PDI | Size | SD | A | PDI |
| | Microfluidizer | [nm] | [nm] | [%] | - | [nm] | [nm] | [%] | - |
| 4 | 5 Passes | 18.52 | 3.61 | 72.60 | 0.38 | 195.60 | 43.50 | 27.40 | 0.38 |
| 5 | 1 Pass | 18.50 | 3.86 | 44.60 | 0.53 | 141.40 | 32.77 | 55.40 | 0.53 |
| | 2 Passes | 19.51 | 3.14 | 53.60 | 0.47 | 155.60 | 32.48 | 46.40 | 0.47 |
| | 3 Passes | 21.95 | 5.36 | 67.30 | 0.41 | 162.00 | 35.65 | 32.70 | 0.41 |
| | 4 Passes | 23.10 | 4.08 | 68.50 | 0.46 | 164.00 | 35.06 | 31.50 | 0.46 |
| | 5 Passes | 19.28 | 3.30 | 74.80 | 0.37 | 225.20 | 47.33 | 25.20 | 0.37 |
| 6 | 1 Pass | 12.76 | 1.87 | 42.10 | 0.74 | 159.50 | 38.19 | 57.90 | 0.74 |
| 7 | 2 Passes | 12.53 | 2.32 | 56.70 | 0.56 | 154.80 | 40.46 | 43.30 | 0.56 |
| 8 | 3 Passes | 11.92 | 2.06 | 52.40 | 0.60 | 149.30 | 38.23 | 47.60 | 0.60 |
| 9 | 4 Passes | 12.56 | 2.12 | 55.30 | 0.48 | 140.10 | 31.67 | 44.70 | 0.48 |

***Table A 9:*** **Zeta-potential of microfluidized rhodamine B liposomes**

| | | Zeta-Potential | |
|---|---|---|---|
| Batch | Processing | Mean charge | SD |
| | Microfluidizer | [mV] | [mV] |
| 4 | 5 Passes | 40.60 | 3.68 |
| 5 | 1 Pass | 20.30 | 2.88 |
| | 2 Passes | 22.50 | 2.42 |
| | 3 Passes | 18.70 | 2.45 |
| | 4 Passes | 12.00 | 1.82 |
| | 5 Passes | 24.00 | 1.62 |
| 6 | 1 Pass | 38.70 | 3.03 |
| 7 | 2 Passes | 30.10 | 0.65 |
| 8 | 3 Passes | 32.70 | 2.56 |
| 9 | 4 Passes | 29.70 | 1.57 |

***Table A 10:*** **Size and size distributions of curcumin liposomes after processing with a microfluidizer**

| | | Peak 1 | | | |
|---|---|---|---|---|---|
| Batch | Processing | Mean Size | SD | A | PDI |
| | Microfluidizer | [nm] | [nm] | [%] | - |
| 1 | 1 Pass | 74.36 | 16.14 | 100.00 | 0.25 |
| 2 | 1 Pass | 72.63 | 15.56 | 100.00 | 0.26 |
| 3 | 1 Pass | 80.15 | 15.00 | 100.00 | 0.21 |

***Table A 11:*** **Zeta potential of Curcumin liposomes after one pass on a microfluidizer**

| | | Zeta-Potential | |
|---|---|---|---|
| Batch | Processing | Mean charge | SD |
| | Microfluidizer | [mV] | [mV] |
| 1 | 1 pass | -1.67 | 1.48 |
| 2 | 1 pass | -1.52 | 1.56 |
| 2 | 1 pass | -2.93 | 1.43 |

***Table A 12:*** **Size and size distributions of empty PEGylated liposomes after one pass on a microfluidizer**

| | | Peak 1 | | | |
|---|---|---|---|---|---|
| Batch | Processing | Mean Size | SD | A | PDI |
| | Microfluidizer | [nm] | [nm] | [%] | - |
| 1 | 1 Pass | 170.70 | 39.74 | 100.00 | 0.30 |
| 2 | 1 Pass | 176.70 | 48.57 | 100.00 | 0.30 |

***Table A 13:*** **Zeta-potential of empty PEGylated liposomes after one pass on a microfluidizer**

| | | Zeta-Potential | |
|---|---|---|---|
| Batch | Processing | Mean charge | SD |
| | Microfluidizer | [mV] | [mV] |
| 1 | 1 pass | -40.00 | 3.88 |
| 2 | 1 pass | -38.70 | 6.74 |

***Table A 14:*** **Size and size distributions of empty liposomes after one pass on a microfluidizer**

| | | Peak 1 | | | | Peak 2 | | | |
|---|---|---|---|---|---|---|---|---|---|
| Batch | Processing | Size | SD | A | PDI | Size | SD | A | PDI |
| | Microfluidizer | [nm] | [nm] | [%] | - | [nm] | [nm] | [%] | - |
| 1 | 1 Pass | 31.49 | 6.28 | 41.40 | 0.47 | 168.60 | 58.60 | 0.467 | 0.47 |
| 2 | 1 Pass | 27.84 | 4.48 | 39.50 | 0.49 | 147.20 | 33.90 | 60.50 | 0.49 |
| 3 | 15s + 1 Pass | 95.77 | 24.00 | 100.00 | 0.24 | - | - | - | - |

***Table A 15:*** **Zeta-potential of empty PEGylated Curcumin liposomes after one pass on a microfluidizer**

| | | Zeta-Potential | |
|---|---|---|---|
| Batch | Processing | Mean charge | SD |
| | Microfluidizer | [mV] | [mV] |
| 1 | 1 Pass | -22.30 | 3.18 |
| 2 | 1 Pass | -33.80 | 6.29 |
| 3 | 1 Pass | -17.40 | 2.98 |

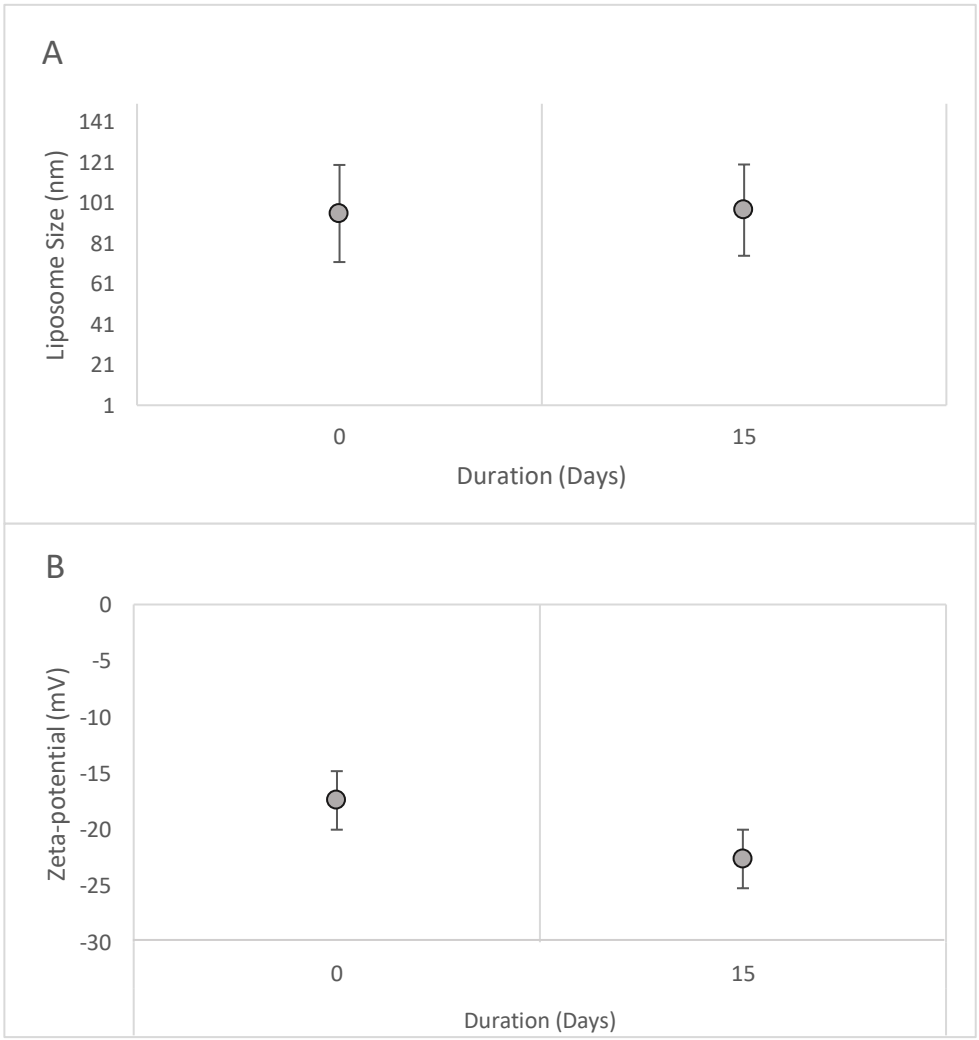


***Figure A 1****: Changes in size (A) and zeta-potential (B) between day 0 and 15 of PEGylated curcumin liposomes passed once on a microfluidizer.*